FBXW7 influences murine intestinal homeostasis and cancer, targeting Notch, Jun, and DEK for degradation

Roya Babaei-Jadidi,[1,2,3] Ningning Li,[1,2,3] Anas Saadeddin,[1,2,3] Bradley Spencer-Dene,[4] Anett Jandke,[5] Belal Muhammad,[1,2,3] ElSayed E. Ibrahim,[1,2,3] Ranjithmenon Muraleedharan,[1,2,3] Mohammed Abuzinadah,[1,2,3] Hayley Davis,[6] Annabelle Lewis,[6] Susan Watson,[2,3] Axel Behrens,[5] Ian Tomlinson,[6] and Abdolrahman Shams Nateri[1,2,3]

[1]Cancer Genetics and Stem Cell Biology Group, [2]Division of Pre-Clinical Oncology; and [3]Nottingham Digestive Diseases Centre Biomedical Research Unit, School of Clinical Sciences, University of Nottingham, Nottingham NG7 2UH, England, UK
[4]Experimental Pathology Laboratory and [5]Mammalian Genetics Laboratory, Cancer Research UK London Research Institute, London WC2A 3PX, England, UK
[6]Molecular and Population Genetics Laboratory, Wellcome Trust Centre for Human Genetics, University of Oxford, Oxford OX3 7BN, England, UK

The Fbxw7 (F-box/WD repeat–containing protein 7; also called CDC4, Sel10, Ago, and Fbw7) component of the SCF (Skp1/Cullin/F-box protein) E3 ubiquitin ligase complex acts as a tumor suppressor in several tissues and targets multiple transcriptional activators and protooncogenes for ubiquitin-mediated degradation. To understand Fbxw7 function in the murine intestine, in this study, we specifically deleted *Fbxw7* in the murine gut using *Villin*-Cre (*Fbxw7*$^{\Delta G}$). In wild-type mice, loss of Fbxw7 in the gut altered homeostasis of the intestinal epithelium, resulted in elevated Notch and c-Jun expression, and induced development of adenomas at 9–10 mo of age. In the context of APC (adenomatous polyposis coli) deficiency (*Apc*$^{Min/+}$ mice), loss of Fbxw7 accelerated intestinal tumorigenesis and death and promoted accumulation of β-catenin in adenomas at late but not early time points. At early time points, Fbxw7 mutant tumors showed accumulation of the DEK protooncogene. DEK expression promoted cell division and altered splicing of tropomyosin (TPM) RNA, which may also influence cell proliferation. DEK accumulation and altered TPM RNA splicing were also detected in FBXW7 mutant human colorectal tumor tissues. Given their reduced lifespan and increased incidence of intestinal tumors, *Apc*$^{Min/+}$*Fbxw7*$^{\Delta G}$ mice may be used for testing carcinogenicity and drug screening.

CORRESPONDENCE
Abdolrahman Shams Nateri:
a.nateri@nottingham.ac.uk

Abbreviations used: APC, adenomatous polyposis coli; β-gal, β-galactosidase; CBC, crypt base cell; CRC, colorectal cancer; EC, epithelial cell; HA, hemagglutinin; IHC, immunohistochemistry; IP, immunoprecipitation; ISH, in situ hybridization; IVT, in vitro translation; Luc, luciferase; MALDI, matrix-assisted laser desorption/ionization; mRNA, messenger RNA; MS, mass spectrometry; qRT-PCR, quantitative RT-PCR; RT, reticulocyte; SCF, Skp1/Cullin/F-box protein; siRNA, small interfering RNA; TA, transiently amplifying; TPM, tropomyosin.

Adult intestinal epithelium homeostasis occurs through a series of processes, including the intestinal stem cells' self-renewal, proliferation, and differentiation and migration of these cells toward the intestinal epithelium (Crosnier et al., 2006). Both the maintenance of tissue homeostasis and the subsequent development of cancer require the degradation of many proteins via the ubiquitin–proteasome pathway (Hershko and Ciechanover, 1998; Crosnier et al., 2006).

The Fbxw7 (F-box/WD repeat–containing protein 7; Welcker and Clurman, 2008) gene locus encodes three isoforms (α, β, and γ), each of which is translated from a common precursor messenger RNA (mRNA) with a unique 5′ exon and 10/9 shared exons in human/mouse, respectively (Koepp et al., 2001; Strohmaier et al., 2001; Matsumoto et al., 2006). Although Fbxw7-α is detected in all murine tissues, Fbxw7-β is restricted to brain and testis and Fbxw7-γ to heart and skeletal muscles (Matsumoto et al., 2006). Fbxw7 acts

R. Babaei-Jadidi and N. Li contributed equally to this paper.

The Rockefeller University Press $30.00
J. Exp. Med. Vol. 208 No. 2 295-312
www.jem.org/cgi/doi/10.1084/jem.20100830

as a tumor suppressor, and mutations in the *Fbxw7* gene are found in ovarian (Kwak et al., 2005), breast (Cassia et al., 2003; Ekholm-Reed et al., 2004), endometrial (Spruck et al., 2002; Cassia et al., 2003), lymphoma (Rajagopalan et al., 2004), and colorectal (Moberg et al., 2001; Kemp et al., 2005) cancers.

The Fbxw7 protein belongs to the F-box protein family and functions as a receptor subunit for SCF (Skp1/Cullin/F-box protein) E3 ubiquitin ligases (SCF^{Fbxw7}; Welcker and Clurman, 2008). SCF^{Fbxw7} binds and regulates the abundance of proteins in a phosphorylation-dependent manner, as in cyclin E (Koepp et al., 2001), c-Myc (Welcker et al., 2004b), Aurora-A (Mao et al., 2004a), SRC-3 (Wu et al., 2007), SPERB (Sundqvist et al., 2005), PGC-1α (Olson et al., 2008), mTOR (Mao et al., 2008), c-Jun (Nateri et al., 2004), NICD (O'Neil et al., 2007), and Notch (Wu et al., 2001).

As depletion of Fbxw7 in mice leads to embryonic lethality (Tetzlaff et al., 2004; Tsunematsu et al., 2004), it remains largely unclear how Fbxw7 regulates signaling pathways that drive intestinal tissue homeostasis and colorectal cancer (CRC). To investigate the role of Fbxw7 in the intestine, we generated mice with conditional *Fbxw7*-floxed alleles ($Fbxw7^{fl/fl}$), permitting tissue-specific gene inactivation. We conditionally ablated Fbxw7 in the murine intestinal epithelium ($Villin\text{-}Cre^{+}Fbxw7^{fl/fl}$ or $Fbxw7^{\Delta G}$, as *Fbxw7* gut-specific deletion; el Marjou et al., 2004) and in the intestinal cancer mouse model $Apc^{Min/+}$ ($Apc^{Min/+}Fbxw7^{\Delta G}$; Fodde, 2002).

In this study, we report that intestinal Fbxw7 inactivation induces adenomas. $Fbxw7^{\Delta}$ intestinal cells altered Notch and Jun pathways to affect both the fate and the maintenance of progenitor cells and proliferating crypt cells. We identify the protooncogene DEK as a novel target of GSK-3β/SCF^{Fbxw7} ligase activity that changes alternative RNA splicing of tropomyosin (TPM) isoforms. Fbxw7 inactivation impairs degradation of the DEK protooncogene and leads to specific loss of the epithelial isoform of TPM, which, cooperatively with Notch and Jun, contributes to carcinogenesis in mice.

RESULTS

Deletion of *Fbxw7* in the mouse intestine ($Fbxw7^{\Delta G}$) leads to intestinal and colonic polyposis

As Fbxw7-null embryos die in utero (Tetzlaff et al., 2004; Tsunematsu et al., 2004), we generated a conditional transgenic mouse with an *Fbxw7* allele, in which exon 5 (encoding the F-box domain) is floxed (Fig. 1 A and Fig. S1). Bitransgenic $Villin\text{-}Cre^{+}Fbxw^{fl/fl}$ ($Fbxw7^{\Delta G}$) mice were then generated to investigate the role of SCF^{Fbxw7} E3 ligase activity in the intestine (Fig. S1). *Villin*-Cre–mediated (el Marjou et al., 2004) *Fbxw7* deletion efficiently and specifically occurred in the intestine of $Fbxw7^{\Delta G}$ mice compared with $Fbxw^{fl/fl}$ (Fig. 1 B). Immunohistochemistry (IHC) analysis of $Fbxw7^{fl/fl}$ mice showed that nuclear Fbxw7 was widely expressed in the intestinal epithelia, including crypt base cells (CBCs; Fig. 1, C and D, red arrowheads), whereas cytosolic Fbxw7 was hardly detectable (Fig. 1, C and D, black arrowheads). In situ hybridization (ISH) of *Fbxw7* in $Fbxw7^{fl/fl}$ mice showed that *Fbxw7* mRNA was strongly expressed in CBCs and transiently amplifying (TA) cells located in crypts (Fig. 1 I, arrowheads), whereas weaker expression of *Fbxw7* was detected in differentiated villus cells. *Fbxw7* expression was abolished in the $Fbxw7^{\Delta G}$ but not in heterozygous $Fbxw7^{\Delta G/fl}$ mice (Fig. 1, I and J vs. K). Quantitative RT-PCR (qRT-PCR) data also confirmed increased levels of *Fbxw7* mRNA expression in the crypt versus villus fraction (Fig. 1, L).

All of the aforementioned analyses demonstrate efficient deletion of Fbxw7 in $Fbxw7^{\Delta G}$ intestinal epithelia but not for $Fbxw7^{\Delta G/fl}$ heterozygous mice when compared with $Fbxw7^{fl/fl}$ mice (Fig. 1, D vs. F and H, I vs. J and K, and L, right). At 9–10 mo of age, the $Fbxw7^{\Delta G}$ mice showed adenomas and induction of Peyer's patch formation (mean three to five) in the large bowel (Fig. S2). In addition, smaller polyp-like structures and initiation of crypt budding and fission were found in the small intestine (Fig. S2). These observations indicate that high expression of Fbxw7 in CBCs and TA cells located in the crypts may potentially function in intestinal cell linage commitments, and the loss of Fbxw7 in both alleles could be associated with tumorigenesis.

Adenomatous polyps are induced in the intestines of double mutant mice ($Apc^{Min/+}Fbxw7^{\Delta G}$) at an early age

To study the functional importance of Fbxw7 in intestinal tumorigenesis and any potential synergy between Fbxw7 and APC (adenomatous polyposis coli; Fodde, 2002) in orchestrating human oncosuppression, we generated a double mutant mouse line, $Apc^{Min/+}Fbxw7^{\Delta G}$. The $Apc^{Min/+}$ mouse is a model of human familial adenomatous polyposis, bearing a nonsense mutation at codon 850 of the *APC* gene (Fodde, 2002) which, combined with a loss of heterozygosity or promoter hypermethylation, results in ligand-independent activation of the WNT/β-catenin pathway (Kennell and Cadigan, 2009).

$Apc^{Min/+}Fbxw7^{\Delta G}$ mice exhibited rapid tumor development throughout the intestine with clearly discernible $\beta\text{-catenin}^{High}$ macroscopic adenomas versus control $Apc^{Min/+}Fbxw7^{fl/fl}$ mice at 3 wk of age (Fig. 2, A and B; and Fig. S3, A–F). All $Apc^{Min/+}Fbxw7^{\Delta G}$ mice developed adenomas (Fig. 2, A and B; and Fig. S3, A–F) without discernible metastases and were culled at 3–5 wk of age (Fig. 2 C; $n = 14$; $P < 0.001$). In contrast, single *Fbxw7* deletion compromised survival in mice, with 42% of the $Fbxw7^{\Delta G}$ mice dying after 11–12 mo versus the control $Fbxw7^{fl/fl}$ (Fig. 2 C; $n = 14$). With a 21 ± 3 wk of maximal mean lifespan (Fig. 2 C; $n = 14$), both control $Apc^{Min/+}Fbxw7^{fl/fl}$ and $Apc^{Min/+}Fbxw7^{+/+}$ yield a very few small-sized polyps without macroscopic adenomas at 3 wk of age (Fig. S4, A–D). The low frequency of $\beta\text{-catenin}^{High}$ adenomas from $Apc^{Min/+}Fbxw7^{fl/fl}$ and $Apc^{Min/+}Fbxw7^{+/+}$ (Fig. S4, A–D) was quantified versus $Apc^{Min/+}Fbxw7^{\Delta G}$ mice (Fig. 2 D; $P \leq 0.001$). Epithelial β-catenin expression remained unchanged at 1 and 3 d postpartum in the $Apc^{Min/+}Fbxw7^{\Delta G}$ versus the control $Apc^{Min/+}Fbxw7^{fl/fl}$ mice (Fig. S4, G and H vs. E and F).

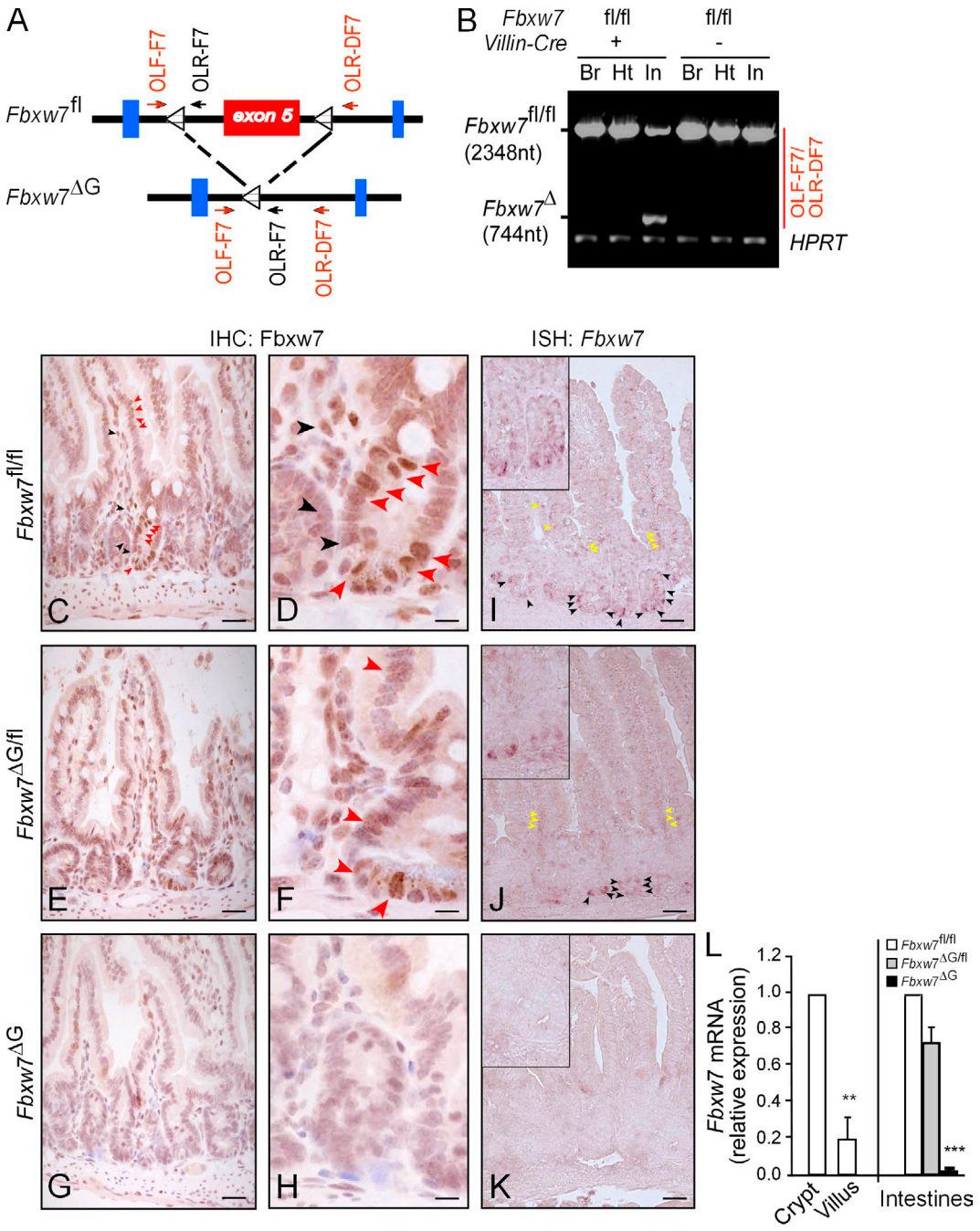

Figure 1. Targeted gene deletion of Fbxw7 in mouse intestine. (A) Schematic shows the floxed *Fbxw7* allele (*Fbxw7*$^{fl/fl}$) before and after *Cre* recombination to generate gut-specific conditional *Fbxw7* inactivation (*Fbxw7*$^{\Delta G}$) mice. Arrows indicate location of PCR primers (black, LoxP; and red, *Fbxw7*) used. (B) PCR analysis of genomic DNA from brain (Br), heart (Hr), and intestine (In) from *Fbxw7*$^{fl/fl}$ and *Fbxw7*$^{\Delta G}$ mice. OLF-F7/OLR-DF7 PCR shows *Fbxw7* gene status. *HPRT* was used as a loading control. (C–H) IHC for Fbxw7 on representative intestinal tissue sections of 6-wk-old *Fbxw7*$^{fl/fl}$ (C and D), *Fbxw7*$^{\Delta G/fl}$ (E and F), and *Fbxw7*$^{\Delta G}$ (G and H) mice. Figures are shown at low magnification (C, E, and G) and at high magnification (D, F, and H). Red arrowheads show cells with nuclear Fbxw7, and black arrowheads show cells with cytoplasmic Fbxw7. Experiments were performed for each genotype and for all four different sections (jejunum, ileum, cecum, and colon) and repeated on at least three independent occasions. (I–K) ISH for *Fbxw7* on representative intestinal tissue sections of 6-wk-old *Fbxw7*$^{fl/fl}$ (I), *Fbxw7*$^{\Delta G/fl}$ (J), and *Fbxw7*$^{\Delta G}$ (K) mice. In I and J, yellow arrowheads indicate *Fbxw7*$^{+}$ cells in villi, and black arrowheads indicate *Fbxw7*$^{+}$ cells in crypts. Boxes indicate magnified intestinal crypts. Experiments were performed in duplicate for each genotype and repeated on at least two independent occasions. (L) qRT-PCR analysis of *Fbxw7* mRNA expression in crypts and villi isolated from *Fbxw7*$^{fl/fl}$ intestine and *Fbxw7*$^{fl/fl}$, *Fbxw7*$^{\Delta G/fl}$, and *Fbxw7*$^{\Delta G}$ whole intestines. Data are mean ± SEM ($n = 3$; **, $P < 0.01$; ***, $P < 0.001$). Experiments were performed in triplicate for each genotype and repeated at least on three independent occasions. Bars: (C, E, G, and I–K) 50 µm; (D, F, and H) 10 µm.

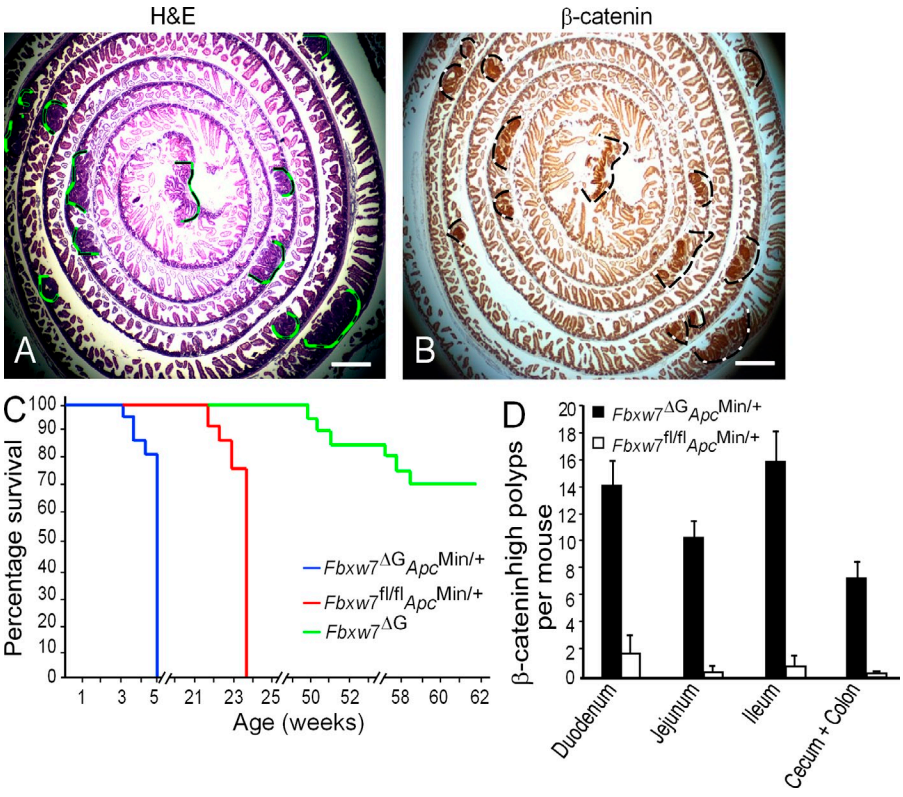

Figure 2. In the *Apc*$^{Min/+}$ mouse, gut-specific conditional *Fbxw7* inactivation (*Apc*$^{Min/+}$*Fbxw7*$^{\Delta G}$ mice) induced tumorigenesis and compromised lifespan and survival. (A and B) H&E staining (A) and IHC for β-catenin (B) on duodenum from 3-wk-old *Apc*$^{Min/+}$*Fbxw7*$^{\Delta G}$ mice. Experiments were performed in duplicate for all four different sections for each genotype and repeated on at least two independent occasions. Dashed lines indicate intestinal polyps and adenomas (A, green) expressing high amounts of β-catenin (B, black). Bars, 100 µm. (C) Kaplan-Meier survival curves for *Fbxw7*$^{\Delta G}$, *Apc*$^{Min/+}$*Fbxw7*$^{fl/fl}$, and *Apc*$^{Min/+}$*Fbxw7*$^{\Delta G}$ mice showing the percentage of mice remaining alive at 1-wk intervals. The x axis indicates times (weeks) until mice were euthanized because of severe weight loss. Groups of 14 mice per genotype were used for analysis, and survival curves were statistically different from each other ($P < 0.001$). (D) β-Catenin polyps (graph shows mean ± SEM) were counted in *Apc*$^{Min/+}$*Fbxw7*$^{fl/fl}$ and *Apc*$^{Min/+}$*Fbxw7*$^{\Delta G}$ mice ($n = 4$ of each genotype according to intestinal locations) on two independent occasions.

Thus, the result suggests that gut-specific *Fbxw7* inactivation in the *Apc*$^{Min/+}$ (*Apc*$^{Min/+}$*Fbxw7*$^{\Delta G}$) mice induces tumorigenesis and compromises lifespan and survival. In addition, loss of *Fbxw7* in the context of *APC* deficiency may accelerate extensive intestinal tumorigenesis in mice without an immediate Wnt/β-catenin activation, at 3 d postpartum but with substantial β-catenin accumulation in adenomas at 3 wk of age. This observation suggests that the accumulation of β-catenin may require additional activators after longer loss of Fbxw7 or APC to cause progressive development of intestinal adenomas (Phelps et al., 2009).

Notch and Jun signaling pathways alter both the fate of progenitor cells and the maintenance of proliferating crypt cells in *Fbxw7*$^{\Delta}$ intestinal cells

To investigate the mechanisms by which mutated Fbxw7 may lead to cancer development, our subsequent analysis was focused on young *Fbxw7*$^{\Delta G}$ mice that showed signs of altered intestinal epithelial cell (EC) composition accompanied by an induction of apoptosis in cells located in crypts positive for active caspase-3 at position 4–5 (Fig. S5, A and B, left vs. right). There was an increase of apoptotic cells by >55% in the small intestine and 30% in the large bowel in the crypts of *Fbxw7*$^{\Delta G}$ mice when compared with floxed mice (Fig. 3 A; data are mean percentage ± SEM; $n = 3$; ≥200 crypts/mouse and for each genotype).

However, *Fbxw7*$^{\Delta G}$ intestines exhibited a significant loss of goblet cells (Fig. S5 C, left vs. right), along with significantly fewer Paneth and enteroendocrine cells in the *Fbxw7*$^{\Delta G}$ small intestine (Fig. S5 D, left vs. right; and not depicted). Absorptive enterocytes remained unchanged. To further characterize which epithelial lineages may be involved in tumorigenesis, intestinal sections were stained with the goblet cell marker Mucin 2 (Allen et al., 1998), which showed a remarkable reduction in Muc2 secretory cells in *Fbxw7*$^{\Delta G}$ mice (Fig. S5 E, left vs. right).

We next examined the effects of Fbxw7 depletion on intestinal cell division using the proliferation marker Ki67. Mutant mice showed a marked increase in proliferating cells from all intestinal crypts (Fig. 3 B; data are mean ± SEM; $n = 3$; ≥100 crypts per mouse and for each genotype; and Fig. S5 F, left vs. right).

Given these findings, we sought to define the molecular links between Fbxw7 loss and consequent changes in intestinal epithelium. The level of intestinal β-catenin staining was unchanged in either *Fbxw7*$^{\Delta G}$ or the control *Fbxw7*$^{fl/fl}$ mice at 5–6 wk (Fig. S5 G, left vs. right). Next, we analyzed several oncogenic proteins of known Fbxw7 targets by IHC. Staining for Notch 1 (Fig. S5 H, left vs. right) and Notch 4 (Fig. S5 I, left vs. right) showed clearly different expression pattern in the *Fbxw7*$^{\Delta G}$ CBCs and in *Fbxw7*$^{fl/fl}$, respectively. c-Jun was detected in the CBCs and at the apex of the villi (Fig. S6, A and B) and accumulated within the TA cells in *Fbxw7*$^{\Delta G}$ versus *Fbxw7*$^{fl/fl}$ (Fig. S5 J, left vs. right). These observations indicate that depletion of Fbxw7 may cause Notch and c-Jun activation in progenitor cells. This view is supported by Western blotting, which also confirmed that the expression levels of Notch 1, Notch 4, and phosphorylated c-Jun

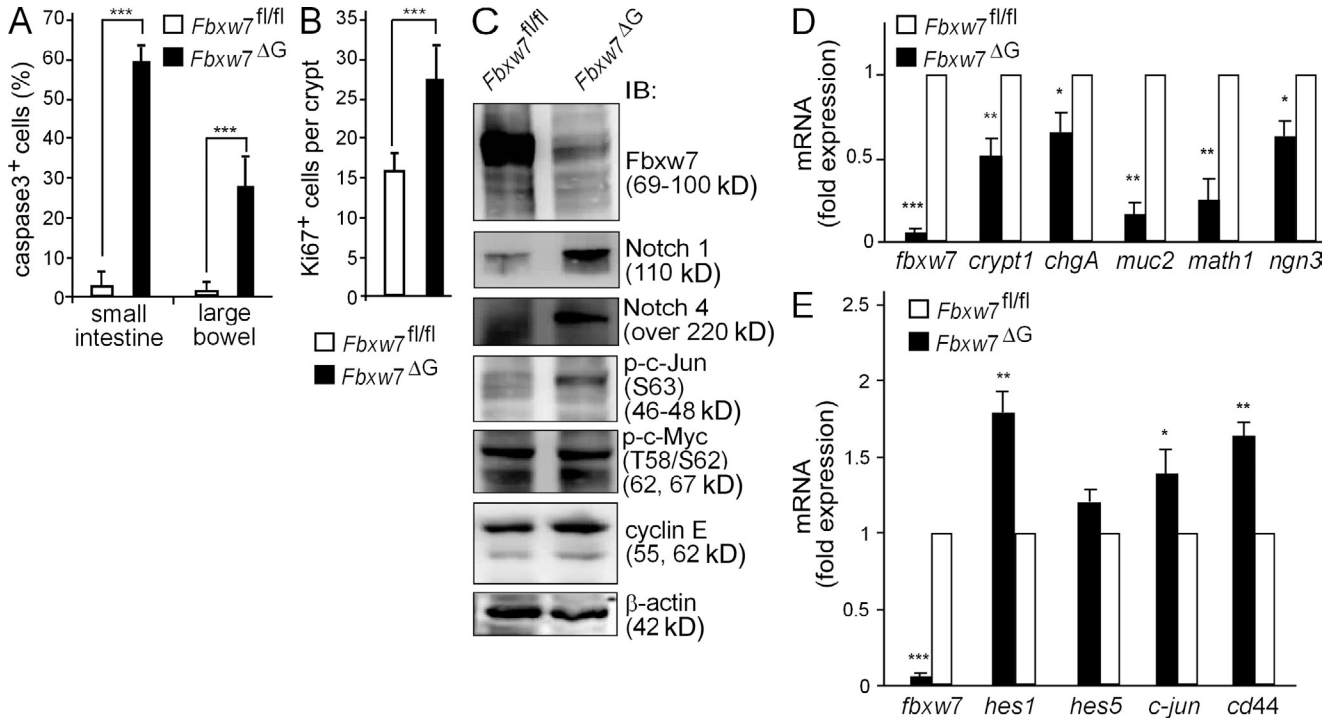

Figure 3. Protein expression of Fbxw7 substrates and mRNA levels of genes responsible for intestinal differentiation, proliferation, and progenitor markers are altered in *Fbxw7*$^{\Delta G}$ intestinal ECs. (A) The mean percentage of caspase-3$^+$ cells (±SEM) in crypts of *Fbxw7*$^{fl/fl}$ and *Fbxw7*$^{\Delta G}$ mice ($n = 3$ for each genotype; 200 crypts each; ***, $P < 0.001$). (B) Ki67-stained cells in crypts of *Fbxw7*$^{fl/fl}$ and *Fbxw7*$^{\Delta G}$ mice ($n = 3$ for each genotype; 100 crypts each) according to intestinal locations. Data present mean per crypt ± SEM ($n = 3$; ***, $P < 0.001$). (C) Western blot analysis of *Fbxw7*$^{fl/fl}$ and *Fbxw7*$^{\Delta G}$ intestinal proteins using antibodies against Fbxw7, Notch 1, Notch 4, p-c-Jun, p-c-Myc, cyclin E, and the loading control β-actin. Experiments were performed on at least two independent occasions. IB, immunoblot. (D and E) qRT-PCR analysis of mRNA encoding the indicated genes responsible for intestinal differentiation, proliferation, and marking progenitors in *Fbxw7*$^{\Delta G}$ and *Fbxw7*$^{fl/fl}$ intestine. Results were normalized to β-actin in the same sample, and data are presented as fold induction/repression over *Fbxw7*$^{fl/fl}$ mice. Mean ± SD ($n = 3$; *, $P < 0.05$; **, $P < 0.01$; ***, $P < 0.001$). Experiments were performed in triplicate for each genotype and repeated on at least three independent occasions.

(p–c-Jun) are increased in *Fbxw7*$^{\Delta G}$ versus *Fbxw7*$^{fl/fl}$ intestine, whereas cyclin E and p–c-Myc are less affected (Fig. 3 C).

Consistent with our observed changes in secretory cell differentiation, the Paneth cell marker *crypt-1* (*cryptidin-1*), the enteroendocrine cell marker *chgA* (*chromogranin A*), and the goblet cell marker *muc2* (*mucin 2*) were reduced in *Fbxw7*$^{\Delta G}$ intestines (Fig. 3 D). To evaluate the role of Notch and c-Jun signal activation on the differentiation and proliferation of intestinal ECs (Fig. S5, A–E), we measured the relative mRNA expression of several Notch/Jun downstream targets by qRT-PCR (Table S1). In general, intestinal expression levels of *Hes-1* (*hairy and enhancer of split 1*), *c-jun*, and *cd44* were increased, whereas the level of *Hes-5* was not significantly affected (Fig. 3 E). Expression of secretory progenitor markers *Math-1* (*mouse atonal homologue 1*) and *ngn-3* (*neurogenin-3*) were also significantly repressed (Fig. 3 D).

Hes-1 expression is transcriptionally activated by Notch and is considered the canonical Notch downstream target gene (Jarriault et al., 1995). Hes-1 deletion led to excessive numbers of goblet, enteroendocrine, and Paneth cells. *Hes-1*$^{-/-}$ mice showed no changes in intestinal proliferation; the up-regulation of *Hes-1* resulted in the repression of *ngn-3* and *Math-1* (Yang et al., 2001), providing further evidence of the effect of Notch overactivation on the differentiation of *Fbxw7*$^{\Delta G}$ intestinal secretory precursor cells. Mice lacking *Hes-1*, *Math-1*, and *ngn-3* show a reduction of goblet, Paneth, and enteroendocrine cells, which may indicate a common progenitor cell for these secretory cell lineages (Jensen et al., 2000; Yang et al., 2001; Jenny et al., 2002).

In the large bowel, CD44 protein expression is normally restricted to the crypt compartment, and expression of *cd44* from *Fbxw7*$^{\Delta G}$ mice was significantly increased (Fig. 3 E and Fig. S5 K, left vs. right). CD44 is a c-Jun target, and it is induced in intestinal tumors (Nateri et al., 2005; Van der Flier et al., 2007). However, induction of CD44 may change the proliferative status of the intestinal progenitor cells when Fbxw7 is inactivated (Fig. S5 F, left vs. right).

Proteomic analysis identified induction in the level of the DEK protooncogene and high molecular weight TPM isoform in *Fbxw7*$^{\Delta}$ intestine

Because β-catenin may not been involved in the early events of intestinal cancer initiation in our mutant mice (Fig. S4, E–H; and Fig. S5 G, left vs. right), we examined whether

other cell regulators can be involved at these earlier stages. Proteins either absent in control *Fbxw7*$^{fl/fl}$ or differentially expressed in *Fbxw7*$^{\Delta G}$ intestines were identified from cytosolic (Fig. 4, A vs. C) and nuclear (Fig. 4, E vs. G) protein extracts using two-dimensional matrix-assisted laser desorption/ionization (MALDI)–mass spectrometry (MS) assays (Kim et al., 2007). Subsequent amino acid sequencing and bioinformatic analyses identified several proteins known to be involved in carcinogenesis. Among others, we identified different isoforms of TPM α and β mouse proteins with high (Fig. 4 D, yellow circles) and low (Fig. 4, B and D, blue circles) molecular weights (Fig. 4, B vs. D and F vs. H) and also a nuclear phosphoprotein

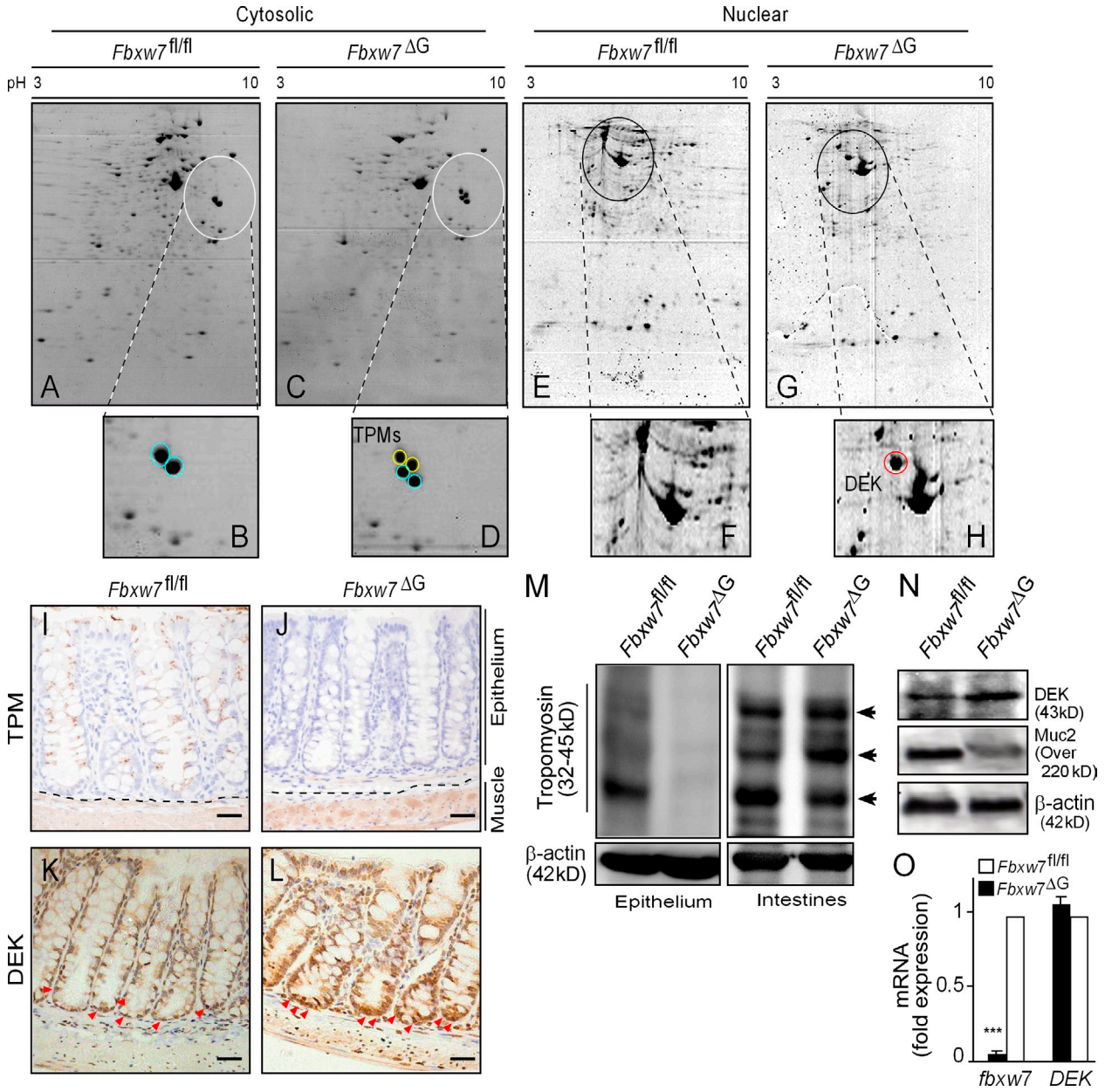

Figure 4. Expression of DEK and TPM is altered in the intestine of *Fbxw7*$^{\Delta G}$ mice. (A–H) Two-dimensional gel/MS-based protein identification using mouse intestinal proteins fractionated into cytosolic (A, *Fbxw7*$^{fl/fl}$; C, *Fbxw7*$^{\Delta G}$) and nuclear extracts (E, *Fbxw7*$^{fl/fl}$; G, *Fbxw7*$^{\Delta G}$). Circled areas in A, C, E, and G are magnified and shown in B, D, F, and H. Blue and yellow circles (B and D) denote isoforms of Tpm; the red circle (H) denotes DEK. (I–L) IHC for TPM and DEK on representative intestinal tissues of 6-wk-old *Fbxw7*$^{fl/fl}$ (I and K) and *Fbxw7*$^{\Delta G}$ mice (J and L). Dashed lines indicate the boundary of the muscle and epithelia. Arrowheads denote DEK-expressing cells. Bars, 50 µm. (M) Western blot analysis of TPMs in epithelia-enriched and whole intestine protein samples from *Fbxw7*$^{fl/fl}$ and *Fbxw7*$^{\Delta G}$ mice. Arrows indicate possible transition of TPM isoforms. (N) Western blot analysis of *Fbxw7*$^{fl/fl}$ and *Fbxw7*$^{\Delta G}$ intestines with DEK, Muc2, and β-actin (loading control) antibodies. (O) qRT-PCR analysis of DEK mRNA in the intestine of *Fbxw7*$^{\Delta G}$ and *Fbxw7*$^{fl/fl}$ mice. Results were normalized to β-actin expression in the same sample, and data are presented as fold over *Fbxw7*$^{fl/fl}$ mice (mean ± SD; $n = 3$; ***, $P < 0.001$). Experiments were performed in triplicate for each genotype and repeated on at least three independent occasions.

DEK (Fig. 4 H, red circle), all of which were subsequently verified by Western blotting and IHC on *Fbxw7*$^{fl/fl}$ and *Fbxw7*$^{\Delta G}$ intestines.

TPM is comprised of tissue-specific isoforms, including skeletal muscle, smooth muscle, fibroblast, and epithelial isoforms that range 32–45 kD (Gunning et al., 2005; Helfman et al., 2008). TPM staining of *Fbxw7*$^{fl/fl}$ intestine showed a cytoplasmic pattern in the smooth muscle cells and vesicular staining in apical ECs (Fig. 4 I) in 6-wk-old mice. In contrast, less apical epithelial staining but stronger staining of the smooth muscle cells was found in the *Fbxw7*$^{\Delta G}$ intestine (Fig. 4 J). Consistent with this, Western blots of TPM on villus-enriched fractions showed a remarkable reduction in the level of epithelial isoforms (Fig. 4 M, left), whereas TPM on whole intestine (epithelia and muscles) showed an increase in the higher molecular weight isoform (Fig. 4 M, right). The finding shows a remarkable transition of TPM protein isoforms in the *Fbxw7*$^{\Delta G}$ compared with control *Fbxw7*$^{fl/fl}$ intestine.

We next examined which Fbxw7 isoform regulates the E3 ligase activity toward TPM degradation and found that the level of overexpressed TPM1-α protein (Houle et al., 2007) was not affected by overexpression of the FBXW7 isoforms in human CRC HCT116 cells (Fig. S7 A). These data suggest that Fbxw7 may not directly influence the TPM protein level but may indirectly affect *TPM* alternative splicing (Gooding and Smith, 2008).

DEK (Fig. 4 H), a nuclear phospho-protooncogene protein, is implicated in carcinogenesis and up-regulated in a variety of aggressive human tumors (Waldmann et al., 2004; Carro et al., 2006). IHC analysis demonstrated intense staining of DEK in crypt cells from *Fbxw7*$^{\Delta G}$ intestine (Figs. 4, K vs. L, arrowheads), and Western blotting also confirmed an increased level of DEK in *Fbxw7*$^{\Delta G}$ intestine (Fig. 4 N). We measured relative *DEK* expression with real-time qRT-PCR (Table S1) and found that DEK mRNA expression was normal (Fig. 4 O). These data suggest that loss of SCF^{Fbxw7} E3 ligase activity can result in the accumulation of DEK protein level.

DEK and TPM expression is associated with the early transformed phenotype in *Apc*$^{Min/+}$*Fbxw7*$^{\Delta G}$ mice

β-Catenin levels in the epithelia of *Apc*$^{Min/+}$*Fbxw7*$^{\Delta G}$ and control *Apc*$^{Min/+}$*Fbxw7*$^{fl/fl}$ mice at early age (3 d postpartum) do not show an apparent difference (Fig. S4, F vs. H); indeed, IHC analysis detected transformation of TPM isoform composition from the epithelial isoform in *Apc*$^{Min/+}$*Fbxw7*$^{fl/fl}$ mice to the muscle isoform in *Apc*$^{Min/+}$*Fbxw7*$^{\Delta G}$ mice 3 d postpartum (Fig. 5, A vs. B, arrowheads). Results also showed a high level of DEK in the intestines of *Apc*$^{Min/+}$*Fbxw7*$^{\Delta G}$ mice 3 d postpartum (Fig. 5, C vs. D). Highly elevated DEK levels were also observed in adenomas of adult double mutant mice (unpublished data). Therefore, we investigated whether DEK and TPM play a role in the regulation of cell growth.

Comparable IHC analysis on wild-type FBXW7 (FBXW7^{wt}) and FBXW7 mutated (FBXW7^{mut}) human colorectal tumors tissues revealed that TPM and DEK expressions in ECs are correlated with FBXW7 mutations in human colon cancer (Fig. 5, E–N; and Tables S2 and S3). TPM expression was elevated in smooth muscle (stromal) cells from FBXW7^{mut} tumors when compared with FBXW7^{wt} tumors (Fig. 5, H vs. L). Quantification data, consistent with our mouse model observation, show that TPM expression in epithelia decreased with FBXW7 mutation (Table S3; $P = 0.0024$), whereas its expression was elevated in stroma compared with FBXW7^{wt} tumors (Table S3; $P = 0.0106$; and Table S2). DEK staining was more intense in FBXW7^{mut} ECs (Fig. 5, J vs. N), revealing its high levels of expression in FBXW7^{mut} tumor tissues (Table S3; $P = 0.0010$).

Notably, lower expression of TPM expression is correlated with a high level of DEK expression in ECs (Fig. 5, H vs. J and L vs. N). Collectively, these data show that accumulation of DEK and loss of epithelial TPM may contribute to the oncogenicity of FBXW7 mutation in both human CRC and in the *Apc*$^{Min/+}$*Fbxw7*$^{\Delta G}$ mouse intestine, which is indicative of possible roles for DEK and TPM in colorectal tumorigenesis (Prasad et al., 1993; Bharadwaj and Prasad, 2002; Mlakar et al., 2009; Wise-Draper et al., 2009).

To test whether there was a functional relationship between CRC cell proliferation and their FBXW7 status, single HCT116 cells lacking or expressing FBXW7 (Mao et al., 2004a; Mao et al., 2008), HCT116$^{-/-}$, HCT116$^{+/-}$, and HCT116$^{+/+}$ cells, were cultured for colony forming assays (Fig. S8 A). Both CRC HCT116$^{+/-}$ and HCT116$^{-/-}$ cell lines, harboring deletion of FBXW7 caused an increase in size and number of cell colonies (Fig. 5 O; $0.0001 < P < 0.05$). In separate tissue culture studies, we investigated the role that TPM may play in CRC cells. Expression of TPM1-α is widely distributed in both smooth muscle cells and the cytoskeleton of ECs (Gunning et al., 2005; Helfman et al., 2008). Therefore, the effects of TPM expression on proliferation, cell migration, and wound healing were then tested in both HCT116$^{+/+}$ and HCT116$^{-/-}$ cells. Both cells were thus transfected with FLAG–TPM1-α and compared with pcDNA backbone vector (control)–transfected cells (Fig. S8 B). We observed that ectopic expression of TPM1-α increased cell number in G0/G1 phase and decreased the number of cells in S phase in both HCT116$^{-/-}$ and HCT116$^{+/+}$ cells (Fig. 5 P; $0.0001 < P < 0.001$). A wound healing assay using the aforementioned transfection protocol in both cells lines (HCT116$^{-/-}$ and HCT116$^{+/+}$) was performed, in which overexpression of TPM1-α repressed wound healing (Fig. 5 Q; $0.0001 < P < 0.05$; and Fig. S8 C). Transfection of FLAG–TPM1-α significantly reduced HCT116$^{+/+}$ ($P < 0.001$) and HCT116$^{-/-}$ cell motility in trans-well migration assay ($P = 0.043$). Western blotting analyses suggest that ectopic expression of TPM1-α in both HCT116$^{-/-}$ and HCT116$^{+/+}$ cells led to an increased level of E-cadherin (Fig. S8 B), which is suggestive of wound healing and cell migration repression (Fig. 5, Q and R). We also found that c-Jun protein levels were decreased in cells transfected with TPM1-α (Fig. S8 B), which is a plausible functional correlation to reduced cell proliferation (Fig. 5 P).

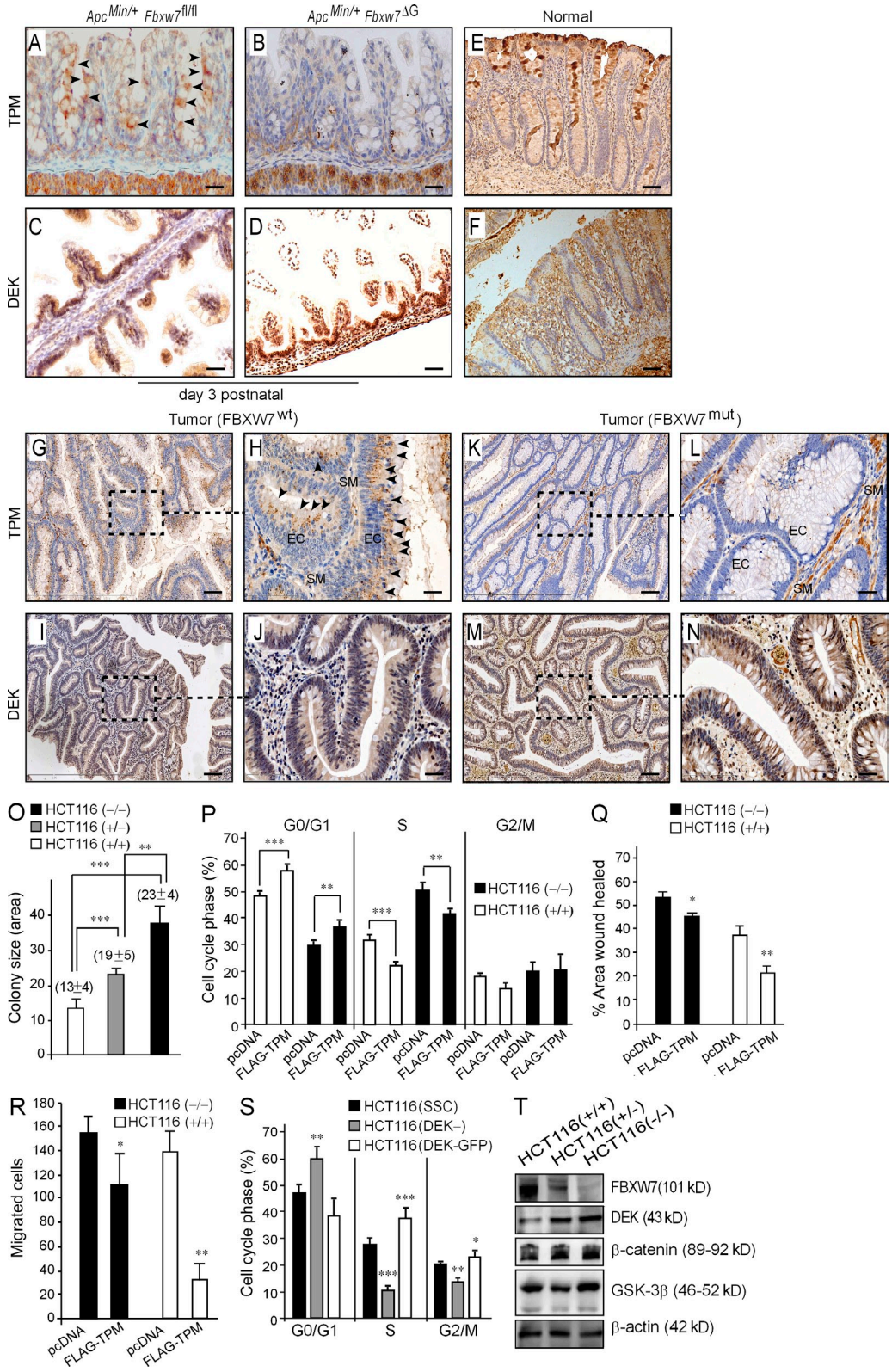

Figure 5. TPM abolishment in epithelium and DEK accumulation in crypt of *Apc*$^{Min/+}$*Fbxw7*$^{\Delta G}$ mice and human colorectal tumors. (A–D) The expression pattern of DEK and TPM of day 3 postnatal *Apc*$^{Min/+}$*Fbxw7*$^{fl/fl}$ (A and C) and *Apc*$^{Min/+}$*Fbxw7*$^{\Delta G}$ (B and D) intestinal tissues. Dashed lines indicate the boundary of the muscle and epithelia. (E–N) IHC for TPM and DEK on representative human colorectal tissues. (E and F) IHC for TPM and DEK in representative sections of normal human colorectal tissues. (G–N) IHC for TPM and DEK in sections of human colorectal tumors with and without FBXW7

We then tested whether DEK induces CRC cell division. HCT116 cells were transfected with the GFP-DEK expression vector (HCT116$^{GFP\text{-}DEK}$) and DEK-specific duplex small interfering RNA (siRNA; HCT116^{DEK-}), and cell cycles were compared with cells transfected with sequence scrambled control siRNA (control; HCT116^{ssc}). Two different siRNA duplexes were used, and down-regulation of DEK was similar (Fig. S8 D). DEK knockdown significantly increased cell number in G0/G1 phase ($P < 0.001$) and decreased the number of cells in S phase (Fig. 5 S, gray bars). In contrast, ectopic expression of GFP-DEK increased the number of cells forming the S-phase plateau (HCT116$^{GFP\text{-}DEK}$ vs. HCT116^{ssc}; $P < 0.001$) as well as the G2/M-phase peak (HCT116$^{GFP\text{-}DEK}$ vs. HCT116^{ssc}; $P < 0.05$; Fig. 5 S, gray bars), thus suggesting that DEK might play a role in inducing cell division.

To elucidate whether nuclear accumulation of oncogenic β-catenin in the *Apc*$^{Min/+}$ mice and oncogenic DEK in the *Fbxw7*$^{\Delta G}$ mice cooperate in carcinogenesis as in the *Apc*$^{Min/+}$ *Fbxw7*$^{\Delta G}$ mice, we examined β-catenin levels in human CRC HCT116$^{-/-}$ cells, which harbor deletion of FBXW7 and a β-catenin phosphorylation site mutation. Both β-catenin and DEK protein levels were increased in HCT116$^{-/-}$ cells (Fig. 5 T), suggesting that HCT116$^{-/-}$ cells may mimic the molecular defects of adenomas developed by *Apc*$^{Min/+}$*Fbxw7*$^{\Delta G}$ mice. Fbxw7 and β-catenin coimmunoprecipitation (co-IP) experiments did not show a direct interaction between Fbxw7 and β-catenin proteins overexpressed in HEK293T cells (unpublished data). Thus, SCF^{Fbxw7} E3 ligase activity may not directly influence the level of β-catenin. Therefore, collectively, these observations from the double mutant mice and human CRC tissues and cells support the conclusion that DEK accumulation and TPM suppression could be necessary events for the transformed phenotype.

GSK-3β/ SCF$^{Fbxw7\text{-}\alpha}$ E3 ligase activity regulates DEK degradation

DEK is involved in gene transcription and RNA splice site recognition (Soares et al., 2006). Posttranslational modifications play an important role in regulating DEK's binding to DNA and chromatin proteins (Alexiadis et al., 2000; Kappes et al., 2004), and the interaction of DEK with U2AF-RNA requires phosphorylation (Soares et al., 2006). DEK is highly phosphorylated by multiple kinases (Kappes et al., 2004; Soares et al., 2006), and sequence comparison reveals that DEK contains phosphorylation motifs similar to the CDC4-phospho-degron described in other Fbxw7 target proteins (Welcker and Clurman, 2008). In particular, DEK protein harbors four GSK-3β phosphorylation clusters (Fig. S7 B), two at the N terminus (Thr^{15} and Thr^{67}) and the other two at the C terminus (S^{169} and S^{227}; Kappes et al., 2004). How DEK protooncogene function and its expression levels are regulated is largely unclear.

In examining which FBXW7 isoform regulates the E3 ligase activity toward DEK degradation, it is apparent that overexpression of the FBXW7 isoforms in a human cell line HEK293T reveals that DEK, in the presence of GSK-3β, is targeted by FBXW7-α and less so by FBXW7-γ and FBXW7-β (Fig. 6, A [lane 1 vs. lanes 2 and 3] and C [lane 2 vs. lane 1]). Overexpression of Fbxw7-α in HEK293T did not alter DEK mRNA levels (unpublished data). Moreover, GFP-DEK$^{\Delta 100}$ (100-aa deletion mutation at N terminus of DEK protein) co-overexpressed with FBXW7-α was unchanged (Fig. S7 C). Indeed, phosphorylation occurs at the N terminus of DEK protein upon in vitro translation (IVT) of DEK(1–100) in rabbit reticulocyte (RT) lysates, which was observed with higher electrophoretic mobility and treatment of RT lysates containing p-DEK with λ-phosphatase, resulting in an unphosphorylated, faster-migrating form (Fig. 6 B, top). Consistent with this, previous data also confirmed N-terminal DEK phosphorylation by in vitro kinase assays in which DEK was translated in vitro in RT lysates (Soares et al., 2006).

Mutations at either Thr^{15} or Thr^{67} also did not stabilize DEK (unpublished data). In contrast, both phosphorylation clusters of DEK mutant protein (DEK^{T15,67A} or DEK^{2A}; Fig. 6 B, bottom) are similar in the presence or absence of FBXW7-α (Fig. 6 C, lanes 4 and 5), suggesting that both N-terminal phosphorylation clusters at Thr^{15} and Thr^{67} contribute to recognition of DEK by SCF$^{FBXW7\text{-}\alpha}$ for degradation. Blocking phosphorylation and inhibition of GSK-3β expression using LiCl or proteasome inhibitor–stabilized p-DEK (Fig. 6 C, lanes 3 and 6 vs. lane 2). p-DEK was stable in HEK293T cells (Soares et al., 2006), but coexpression of FBXW7 decreased the steady-state levels of DEK and resulted in reduced protein half-life (Fig. 6 D; Nateri et al., 2004). In contrast, the stability of DEK^{2A} mutant protein was not affected in the presence of Fbxw7 (Fig. 6 D). These data suggest that the E3 ligase SCF$^{Fbxw7\text{-}\alpha}$ degrades p-DEK in a GSK-3β–dependent manner. Consistent with this, HCT116$^{-/-}$

mutations. H, J, L, and N show magnified versions of the boxed regions in G, I, K, and M. (A and H) Arrowheads indicate TPM^{+} cells. SM, smooth muscle cell. (O) HCT116 human CRC cells expressing the indicated FBXW7 genotypes were cultured in vitro. Graph shows mean ± SEM, and numbers in parentheses indicate the number of colonies generated from 50 cells seeded in 24-well dishes in triplicate and on two independent experiments. (P–R) FLAG–TPM1-α or control vector (pcDNA) was expressed in HCT116$^{+/+}$ and HCT116$^{-/-}$ cells, and status was monitored for cell cycle via flow cytometry and propidium iodide staining (P). Wound healing (Q) and cell migration (R) were also performed. For quantification of colony area and wound healing, images of wounds and colonies were converted into binary images using the ImageJ program. (S) Cell cycle status of HCT116 cells transfected with expression vector pGFP-DEK (HCT116$^{GFP\text{-}DEK}$), DEK-specific duplex siRNA (HCT116^{DEK-}), and sequence scrambled control siRNA (HCT116^{ssc}) was monitored via flow cytometry and propidium iodide staining in triplicates. (O–S) Error bars present mean ± SEM of three independent experiments (*, $P < 0.05$; **, $P < 0.01$; ***$P < 0.001$). (T) DEK, FBXW7, GSK-3β, and β-catenin expression was measured by Western blotting. Bars: (A–G, I, K, and M) 50 µm; (H, J, L, and N) 10 µm.

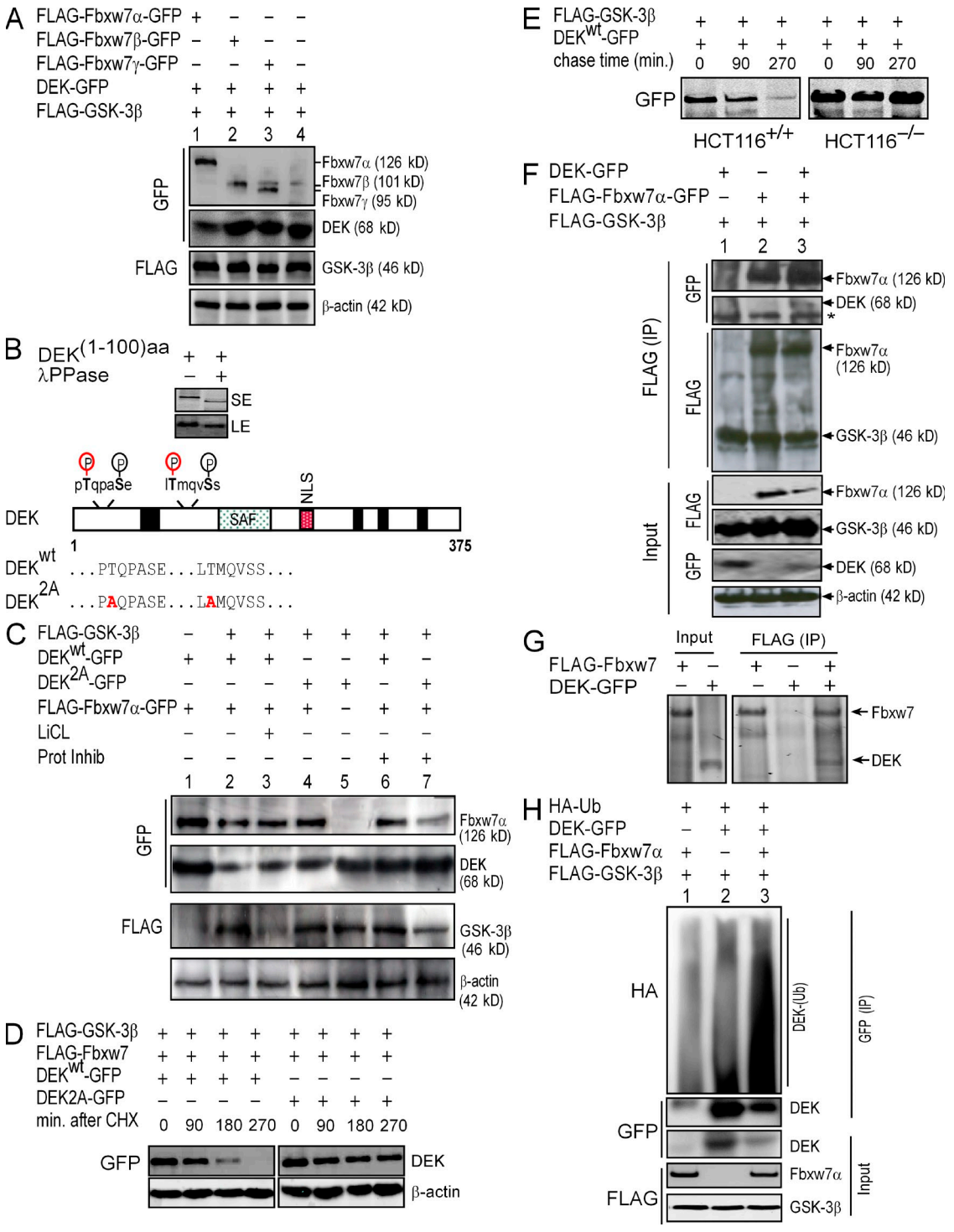

Figure 6. DEK is regulated by the SCF E3 ligase containing the FBXW7-α subunit in a manner dependent on GSK-3β. (A) FLAG-tagged versions of the indicated proteins were expressed in HEK293T cells, and lysates were subjected to immunoblotting with anti-FLAG and anti-GFP. β-Actin was used as a loading control. (B) ^{35}S-labeled DEK was generated by IVT using rabbit RT lysates, with or without λ-phosphatase (λPPase) treatment. Schematic shows potential GSK-3β phosphorylation sites on DEK; red letters document residues mutated in DEK2A. SE, short exposure; LE, long exposure. (C and D) Mutant and wild-type versions of DEK together with other indicated constructs were expressed in HEK293 cells. Cells were treated or not with LiCl and/or proteasome inhibitor I (Prot Inhib) for 8 h (C) or cycloheximide (CHX; D) for the indicated time points. Lysates were examined by Western blotting. (E) HCT116 cells lacking or expressing FBXW7 were transfected with the indicated constructs, labeled with [^{35}S]methionine, and chased with cold methionine for the indicated time points. Lysates were subjected to IP and immunoblotting with anti-GFP. (F) HEK293T cells were transfected with the indicated constructs and subjected to IP and immunoblotting with the indicated antibodies. The asterisk indicates a nonspecific band. (G) FLAG-FBXW7

cells restored the stability of ectopic expression of DEK protein (Fig. 6 E). Therefore, DEK protein level may be directly modulated by $SCF^{Fbxw7\text{-}\alpha}$ E3 ligase activity.

IP of FLAG epitope–tagged FBXW7-α–GFP revealed its interaction with p-DEK–GFP protein (Fig. 6 F, lane 3) in HEK293T cells. Also, IP of in vitro translated FLAG-tagged Fbxw7 showed a direct interaction with the DEK protein (Fig. 6 G). We next examined whether FBXW7 possesses E3 ligase activity toward p-DEK by assessing DEK ubiquitination in HEK293T cells (Wu et al., 2007). DEK was efficiently ubiquitinated (Fig. 6 H, lane 3 vs. lanes 1 and 2), and therefore SCF^{FBXW7} has properties consistent with a function as an E3 ubiquitin ligase that specifically targets p-DEK.

FBXW7-α–mediated degradation of DEK influences *TPM* RNA splicing

Recent experiments have demonstrated that p-DEK influences alternative splicing of RNA (Soares et al., 2006). We examined whether deregulated p-DEK changes alternative RNA splicing of TPM (Fig. 4, I vs. J and M; Gooding and Smith, 2008). We used a double reporter system for determining splicing efficiency (Fig. 7 A; Nasim and Eperon, 2006). A short splicing region containing TPM target intron and its splicing sites (ss) was introduced between two reporters encoding β-galactosidase (β-gal) and luciferase (Luc), such that the upstream β-gal is expressed regardless of splicing (Fig. 7 A). However, the Luc will be expressed unless the multiple stop-codons (reds) residing in the splicing region are removed (Fig. 7 A). Therefore, the proportion of transcript variants can be evaluated by the relative ratio of Luc to β-gal expression.

We show that endogenous p-DEK (Fig. 7 B, lane 1) but not unphosphorylated DEK (Fig. 7 B, lane 5), significantly enhanced the TPM RNA splicing efficiency. A similar observation was made when DEK was overexpressed in the presence and absence of GSK-3β (Fig. 7 B, lane 3 vs. lane 7). Therefore, the phosphorylation of DEK by GSK-3β is a crucial step to mediate Tpm RNA splicing. Intriguingly, p-DEK targeted by FBXW7 significantly reduced the splicing efficiency (Fig. 7 B, lanes 2 and 4 vs. lanes 1 and 3). In addition, the assessment of splicing efficiency by the Luc/β-gal ratio was also independently confirmed by RT-PCR (Fig. 7 C). Consistent with our mouse model (Fig. 4 M), enhanced DEK in $HCT116^{-/-}$ cells is sufficient to facilitate TPM shifts to a higher molecular weight (Fig. 7 D, arrowhead). DEK depletion in $HCT116^{-/-}$ using the DEK-specific duplex siRNA significantly reduced TPM RNA splicing efficiency (Fig. 7 E, left) and also reduced the TPM shifts to the higher molecular weight (Fig. 7 E, right). These data suggest that TPM splicing is directly regulated by GSK-3β/DEK, which in turn is subjected to SCF^{FBXW7} E3 ligase activity.

Intestinal tumorigenesis promoted by the accumulation of proliferating cells in the crypts of $Apc^{Min/+}Fbxw7^{\Delta G}$ mice

Intestinal tumor formation in $Apc^{Min/+}Fbxw7^{\Delta G}$ mice apparently occurs by repopulation of preexisting crypts (unpublished data) with APC mutant cells, as reported for humans (Shih et al., 2001). To determine whether Fbxw7 depletion results in the rapid transformation of intestinal crypt cells into adenomas in $Apc^{Min/+}Fbxw7^{\Delta G}$, we examined the proliferation index of mutants versus litter mate control mice at different ages. Results showed that $Apc^{Min/+}Fbxw7^{\Delta G}$ mice significantly induced proliferation compared with control $Apc^{Min/+}Fbxw7^{fl/fl}$ mice at 3 d postpartum (measurement as $Ki67^+$ cells/micrometer; $P < 0.001$; Fig. 8 A). $Ki67^+$ cells were also significantly increased in $Fbxw7^{\Delta G}$ crypts compared with $Fbxw7^{fl/fl}$ at 3 wk old (measurement as $Ki67^+$ cells/crypt; $P < 0.001$; Fig. 8 B). Further molecular characterization on protein extracts from small intestine isolated at 3 d postpartum indicated that in the $Apc^{Min/+}Fbxw7^{\Delta G}$, the levels of Notch 1, c-Jun, and DEK were significantly increased (Fig. 8 C), similar to the levels present in the $Fbxw7^{\Delta G}$ intestine (Figs. 3 C and 4 N). CyclinD1 protein levels, a positive proliferation marker, were also increased, and TPM protein expression patterns consequently changed (Fig. 8 C). We concluded that $Fbxw7^{\Delta G}$ crypt cells bearing multiple subsequent deregulations in Notch, Jun, and DEK activation result both in early tumor initiation and proliferation and in an increase of tumor incidence at 2–3 wk of age.

DISCUSSION

Despite the well-established links between signaling and transcriptional activity, little is known about how transcriptional activators/repressors are regulated once tumorigenesis has been triggered. One mechanism is by limiting the lifetime of an activator/repressor by destroying it via the ubiquitin–proteasome system (Nakayama and Nakayama, 2006; Welcker and Clurman, 2008). Our study reveals a previously unrecognized role for SCF^{FBXW7} E3 ligase and its substrates in regulating intestinal epithelial homeostasis and tumorigenesis.

In this study, the $Fbxw7^{\Delta G}$ mice at 9–10 mo of age showed adenomas, and crypt budding and fission were also found in the small intestine (Fig. S2). Crypt budding and fission occur in normal intestinal growth and repair as well as in polyposis. It has been suggested that these events occur when the number of intestinal stem cells in a crypt exceeds a threshold (Brittan and Wright, 2002). However, further analysis is required to validate this concept in our mutant mice. Furthermore, inactivation of both *Fbxw7* and *APC* appears to be synergistically accelerating the malignant progress from adenoma to adenocarcinoma (Fig. 2 and Fig. S3).

was generated by IVT, and interaction with DEK-GFP was probed by IP and immunoblotting with the indicated antibodies. (H) HEK293T cells expressing the indicated constructs and HA-tagged ubiquitin (HA-Ub) were subjected to IP and immunoblotting with the indicated antibodies. Experiments in B and E–H and A, C, and D were repeated at least two and three times, respectively.

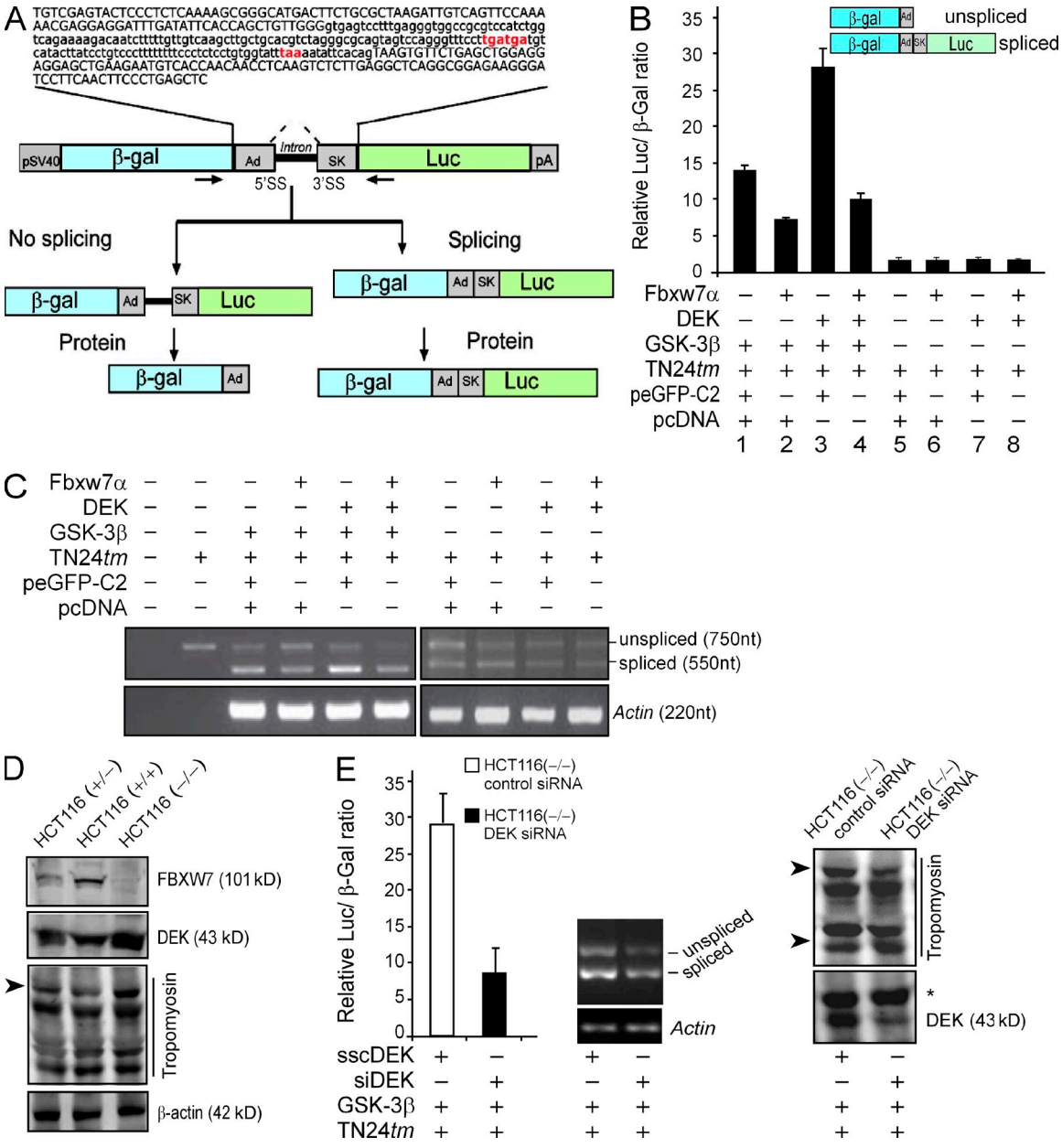

Figure 7. GSK-3β–p-DEK regulates TPM alternative splicing. (A) Schematic of bicistronic reporter construct, TN24tm, used for splicing test. Tpm splicing sites are uppercase and introns are lowercase letters. Splicing and nonsplicing patterns of β-gal and Luc proteins are shown in boxes. Arrows indicate the location of primers for RT-PCR analyses. Red letters indicate stop codons. Ad, adenovirus; pA, poly A signal; SK, skeletal muscle. (B) TN24tm splicing activity assessed by Luc and β-gal expression in HCT116 cells expressing the indicated constructs. Histogram shows the ratio of Luc/β-gal expression (mean ± SEM from three independent experiments). (C) RT-PCR analyses of TN24tm splicing efficiency using RNA from HCT116 cells cotransfected with the indicated constructs. (D) HCT116 cells lacking or expressing FBXW7 were subjected to immunoblotting with the indicated antibodies. The arrowhead marks a higher molecular weight form of TPM. (E) TN24tm splicing assays in HCT116$^{-/-}$ cells transfected with DEK-specific duplex siRNA or scrambled control siRNA. Left panel presents the ratio of Luc/β-gal expression (mean ± SEM from three independent experiments). Middle panel represents the RT-PCR analysis. Right panel shows Western blotting with the indicated antibodies. Arrowheads mark a higher and lower molecular weight form of TPM. The asterisk indicaets a nonspecific band.

Fbxw7$^{\Delta G}$ mice showed activation of Notch, c-Jun, and their downstream targets (Fig. 3 and Fig. S5, G–K). However, our result is consistent with recent reports that activation of the Notch signaling pathways mainly induced *Hes-1* but not *Hes-5* expression; Notch signaling is implicated in the regulation of cell fate specification predominantly by *Hes-1* (Fre et al., 2005; van Es et al., 2005). The induction of *Hes-1* but not *Hes-5* presumably indicates that these genes could be regulated by additional transcription factors as well as Notch and consequently has overlapping but distinct patterns of

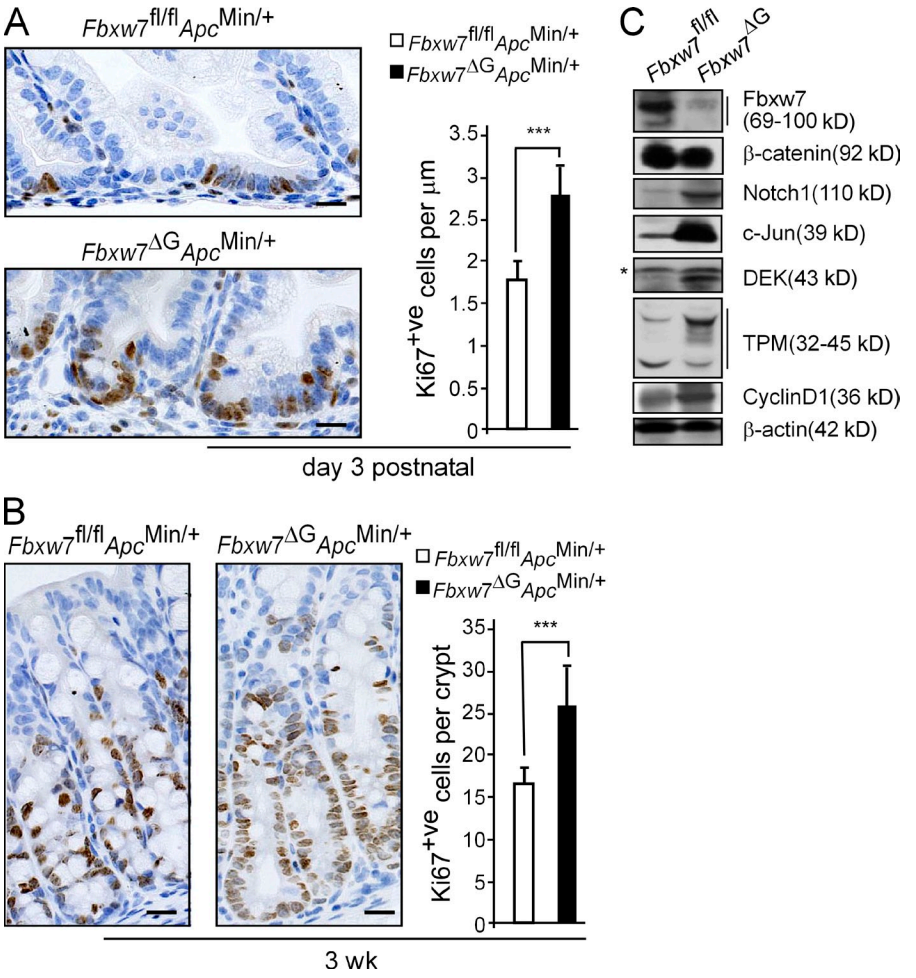

Figure 8. Accumulation of proliferating cells in the crypts of $Apc^{Min/+}Fbxw7^{\Delta G}$ mice. (A and B) IHC for Ki67 expression (left) and quantification of Ki67+ cells (right) from intestines of day 3 postpartum mice (A) or from crypts of 3-wk-old mice (B; >200 crypts in each mouse; $n = 3$ of each genotype). Error bars represent mean ± SEM (***, $P < 0.001$). Bars, 50 µm. (C) Protein extracts from small intestine of 3-d-postpartum mice of indicated genotypes were analyzed by Western blotting. The asterisk indicates a nonspecific band. The experiment was repeated twice.

expression in the gut. Whereas *Hes-1*, *-6*, and *-7* transcripts were apparently restricted to the crypt region, *Hes-5*–expressing cells were also found in the villus epithelium and in the mesenchyme (Schröder and Gossler, 2002). Consistent with previous studies (Schröder and Gossler, 2002; Riccio et al., 2008), Notch 1 was most prominently expressed in ECs of the crypts (Fig. S5 H, left vs. right), where Fbxw7 is also highly expressed (Fig. 1 I), presumably by mediating Notch 1 down-regulation, and consequently *Hes-1* was more affected than *Hes-5*.

We and others have reported that activation of the c-Jun and Notch signaling pathways is implicated in the regulation of cell fate specification and proliferative capacity in the intestine (Fre et al., 2005; Nateri et al., 2005; van Es et al., 2005; Sancho et al., 2009). Our work demonstrates an important role of Fbxw7 in these processes. In addition, *Muc2* expression was also reduced in $Fbxw7^{\Delta G}$ intestines. Collectively, our results (Fig. S5, A–F), along with previous work (Fre et al., 2005; Nateri et al., 2005; van Es et al., 2005; Sancho et al., 2009), suggest that these signals maintain the homeostatic control of intestinal epithelium.

Recent studies have demonstrated that alterations in Notch and c-Jun signals could also be involved in $Fbxw7^{\Delta G}$ intestinal tumorigenesis (Nateri et al., 2005; Akiyoshi et al., 2008; Fre et al., 2009; Sancho et al., 2009). However, Muc2 inactivation also causes intestinal tumor formation (Velcich et al., 2002). Alternatively, expression of the cell cycle regulator cyclin E and the oncogene c-Myc were unaffected by loss of intestinal Fbxw7. Cyclin E expression is not always increased in *Fbxw7*-deficient cells and/or in $Fbxw7^{-/-}$ embryos (Mao et al., 2004b; Rajagopalan et al., 2004; Tsunematsu et al., 2004). In addition, cyclin E levels were not affected in *Fbxw7*-deficient T cells (Onoyama et al., 2007). It is therefore possible that Fbxw7 mediates cyclin E degradation in a tissue-dependent manner. Recent studies have also identified Fbxw7-γ as the major player mediating c-Myc degradation (Welcker et al., 2004a; Bonetti et al., 2008), and it may not be affected in our mice because of the low level of endogenous intestinal Fbxw7-γ isoform expression. Accordingly, we showed that nuclear Fbxw7-α is the major isoform present in intestinal epithelia (Fig. S6 D).

The up-regulation of β-catenin in adenomas from double mutant ($Apc^{Min/+}Fbxw7^{\Delta G}$) mice at 3 wk of age (Fig. 2 and Fig. S3) and in $HCT116^{-/-}$ cells indicates a cross talk between Wnt/β-catenin signaling and FBXW7. However, *Fbxw7*-deleted intestinal epithelia did not lead to a significant accumulation of β-catenin in the intestines of 5/6-wk-old $Fbxw7^{\Delta G}$ mice (Fig. S5 G, left vs. right) and in 3-d-postnatal $Apc^{Min/+}Fbxw7^{\Delta G}$ mice (Fig. S4, F vs. H). We conclude that β-catenin accumulation may require additional factors after prolonged *Fbxw7* or *APC* loss (Phelps et al., 2009).

Although it has already been demonstrated that different TPM isoforms are implicated in neoplastic-specific alterations and that decreased expression of specific nonmuscle TPM isoforms is commonly associated with the transformed phenotype (Helfman et al., 2008), we detected loss of epithelial isoforms of TPM in 3-d-postpartum $Apc^{Min/+}Fbxw7^{\Delta G}$ mice (Fig. 5, A vs. B, arrowheads). Furthermore, a strong

association of epithelial TPM down-regulation in colorectal tumors with FBXW7 mutation (Fig. 5, H vs. L) and our data showing restored expression of TPM1-α in CRC cells (Fig. 5 P) support the conclusion that TPM suppression is required in the sequence leading from FBXW7 depletion to loss of cell growth regulation (Bharadwaj and Prasad, 2002; Varga et al., 2005; Zhu et al., 2007; Zheng et al., 2008; Mlakar et al., 2009). Nevertheless, TPMs exhibit substantial diversity in terms of their size, binding affinity to actin, subcellular localization, and in interactions with other proteins, suggesting that individual TPMs may differ in their biological functions: cell migration and invasion (Miyado et al., 1996; Gunning et al., 2005; Gupton et al., 2005). In parallel to 3-d-postnatal $Apc^{Min/+}Fbxw7^{\Delta G}$ mice (Fig. 5, D vs. C), and in line with a role for DEK in tumorigenesis (Wise-Draper et al., 2009), we also showed that human DEK is highly expressed in human CRC tissues and is correlated significantly with FBXW7 (Fig. 5, N vs. J; and Table S3) mutation and also mediates cell division (Fig. S5). Beyond the current scope of this paper, further contribution of DEK and TPM functions could be compared with other effects of Fbxw7.

Mechanistically, biochemical analysis showed that DEK degradation is mediated by GSK-3β–SCF^{Fbxw7} and that the knockdown or overexpression of Fbxw7 reversibly affects the level of DEK (Figs. 4 and 6). Of note, DEK transcript levels were unchanged, suggesting that DEK is not transcriptionally regulated by activated Notch and/or c-Jun signaling pathways. In addition, we showed that p-DEK changes the alternative RNA splicing of TPM and that the knockdown or overexpression of DEK can be inversely correlated with the levels of different isoforms of TPM (Fig. 7). These findings therefore suggest that aberrant DEK-TPM signaling after loss of the Fbxw7 causes loss of cell growth regulation and consequently, after APC loss and β-catenin accumulation, promote adenoma progression to adenocarcinoma in our double mutant $Apc^{Min/+}Fbxw7^{\Delta G}$ mice. However, further in vivo analysis would be required to validate this concept by genetic intercrosses and generation of Tpm- and/or Dek-deficient mice. Heterozygous deletion of *Fbxw7* in $Fbxw7^{\Delta G/fl}$ mice with no significant abnormality phenotype may phenocopy FBXW7 mutations in human CRC with no loss of a second allele and may function as a haploinsufficient tumor suppressor (Rajagopalan et al., 2004; Kemp et al., 2005). Further analysis, beyond the current scope of this paper, would be required to validate this concept in $Apc^{Min/+}$ mice.

We conclude that Fbxw7 mutation causes failed intestinal differentiation and increased proliferation and occurs in the absence of cyclin E and c-Myc accumulation. Fbxw7 mutation results in accumulation of multiple substrates and in impaired degradation of Notch, Jun, and DEK, which cooperatively contribute to carcinogenesis (Fig. S8 F). Consistent with this model, an intact and functional Fbxw7 is thought to restore homeostatic control mechanisms and impair oncogenic activators. Therefore, strategies based on the partial delivery of Fbxw7-α to intestinal tumor cells would attenuate nuclear DEK and β-catenin accumulation and show promise for fighting colon cancer. Moreover, given the reduced lifespan and increased incidence of intestinal tumors and mortality in $Apc^{Min/+}Fbxw7^{\Delta G}$ mice, these mice could be useful for testing carcinogens and drug screening.

MATERIALS AND METHODS

Mouse lines. Floxed Fbxw7 ($Fbxw7^{fl/fl}$) mice (Fig. S1) were backcrossed a minimum of five times to a C57BL/6 background; *Villin*-Cre transgenic mice (el Marjou et al., 2004) and $Apc^{Min/+}$ mice (Fodde, 2002) were on a C57BL/6 genetic background (Nateri et al., 2005). *Villin*-$Cre^{+}Fbxw7^{fl/fl}$ ($Fbxw7^{\Delta G}$) mice were generated by interbreeding mice carrying $Fbxw7^{fl/fl}$ and the *Villin*-Cre allele. $Apc^{Min/+}Fbxw7^{fl/fl}$ mice were generated by interbreeding mice carrying the floxed alleles of Fbxw7 ($Fbxw7^{fl/fl}$) and $Apc^{Min/+}$, and then $Apc^{Min/+}Fbxw7^{fl/fl}$ were intercrossed with the *Villin*-$Cre^{+}Fbxw7^{fl/fl}$ ($Fbxw7^{\Delta G}$). In all experiments, only littermates were used and compared. Mice were maintained in a specific pathogen-free condition. All experiments were performed at the University of Nottingham in accordance with institutional biomedical service unit guidelines.

Histology and IHC. Intestines were removed, flushed with cold PBS, and processed as "Swiss roll" gut preparations as described previously (Nateri et al., 2005). Tissues were fixed overnight in 10% neutral-buffered formalin, paraffin embedded, and sectioned at 4-μm thickness for hematoxylin and eosin (H&E) staining or IHC with the following primary antibodies: active caspase-3, c-Jun, and p–c-Myc (Cell Signaling Technology); lysozyme, Chromogranin A, and CD44s (Millipore); anti-Ki67 (Dako); Notch 1, Notch 4, and Muc2 (Santa Cruz Biotechnology, Inc.); β-catenin (BD); DEK (Abcam); and Fbxw7 (Thermo Fisher Scientific). Where antigen retrieval was required, slides were microwaved in Na citrate buffer, pH 6, for 12 min. All secondary antibodies were biotinylated (Vector Laboratories), and after incubation with avidin–biotin complex (VectaStain ABC kit; Vector Laboratories), sections were developed with diaminobenzidine. Alkaline phosphatase, periodic acid Schiff (Sigma-Aldrich), and Alcian blue (BDH) were used to identify intestinal cell types according to manufacturers. In adult mice, the Ki67-positive cells per crypt were measured and/or the caspase-3 in 200 full crypts or villi was scored from at least three mice of each genotype. Data for caspase-3 are represented as percentage over control ± SEM. In 3-d-postnatal mice, $Ki67^{+}$ cells were scored from three mice and measured per micrometer, and data are represented in comparison with littermate control ± SEM.

Human CRC specimens from a total of five cases with and six cases without FBXW7 mutations were obtained on separate slides/sections. FBXW7 mutations without loss of heterozygosity were identified by sequencing analysis. Ethical approval and research and development approval were obtained from the Local Research Ethics Committee and the Trust Research and Development office, respectively, in Oxford. For IHC, sections were dewaxed with xylene, rehydrated through graded alcohol, and then boiled in 0.01 M Na citrate buffer, pH 6, for 10 min for antigen retrieval. Immunostaining was performed as outlined above for DEK and TPM antibodies. Staining was evaluated semiquantitatively using an ordinal score scale of 1 = lowest staining and 4 = extensive intense staining. Staining was evaluated independently by four observers. Statistical analysis was performed using SPSS, and FBXW7 statuses were examined for both DEK and TPM for each tumor using the mean of scores ± SD, and a p-value <0.05 was considered statistically significant.

ISH. The mouse Fbxw7 RNA probe was generated from an 800-bp mouse Fbxw7 PCR product (confirmed by sequencing) transcribed with T7 RNA polymerase using the DIG RNA labeling mix (Roche). In brief, 4% PFA-fixed intestinal Swiss roll preparations were sectioned (8 μm), dewaxed, rehydrated, digested with 10 μg/ml proteinase K (37°C for 18 min), and then incubated in 0.2 M HCl and refixed. After prehybridization for 1 h, slides were hybridized overnight at 57°C in buffer containing 50% deionized formamide, 10% dextran sulfate, 1× Denhardt's solution, 10 mM Tris-HCl,

pH 7.6, 600 mM NaCl, 0.25% Na dodecyl sulfate, 1 mM EDTA, 2 mg/ml transfer RNA, and ~2 μg/ml denatured digoxigenin–labeled cRNA probe. The slides were rinsed in 5× SSC at 57°C for 10 min, washed once in 50% formamide in 2× SSC at 57°C for 30 min, and then once in 2× SSC at 57°C for 30 min and twice in 0.2× SSC for 30 min each at 57°C. After blocking with 1% blocking reagent (Roche), slides were incubated with sheep anti-digoxigenin fab antibody (1:1,000; Roche) for 2 h at 37°C. Substrate was developed using NBT/BCIP.

qRT-PCR analysis. For qRT-PCR analysis, total RNA was isolated from freshly dissected intestines using TRIZOL reagent (Sigma-Aldrich) and purified using the RNeasy mini kit including DNase (QIAGEN) according to the manufacturer's instructions. cDNA synthesis was performed using Superscript reagents (Invitrogen) according to the manufacturer's instructions. Quantitative real-time PCR was accomplished with SYBR green incorporation (Platinum Quantitative PCR SuperMix-UDG w/ROX; Invitrogen) using an ABI7900HT (Applied Biosystems), and the data were analyzed using SDS 2.3 software (Applied Biosystems). Results were normalized to those obtained with β-actin, and data are presented as fold induction/repression over control mice. Details of primers used are shown in Table S1. All assays were performed in triplicate at least three times.

Proteomic assays. Intestinal samples from young (≤5 wk) mutant *Fbxw7*$^{\Delta G}$ and control *Fbxw7*$^{fl/fl}$ mice were initially homogenized with ice-cold PBS, and protein extracts were derived following fractionation cytosolic and nuclear extracts according to the manufacturer's instructions (BioVision), resuspended in two-dimensional lysis buffer (Kim et al., 2007), and loaded separately onto Immobiline DryStrip gels containing a preformed pH gradient (pH 3–10), and proteins were run on the Protean IEF Cell (Bio-Rad Laboratories) according to the manufacturer's instructions, separated on a 12% polyacrylamide gel, and then stained with Coomassie blue. Gels were scanned on a calibrated imaging densitometer (GS-800; Bio-Rad Laboratories), and images were analyzed using PDQuest (Bio-Rad Laboratories). All assays were performed at least three times. For an accurate determination of the weight of the novel protein or proteins, MALDI-MS provided by the protein chemistry facility with a Mass-Prep robotic liquid handling system and MALDI TOF mass spectrometer (Waters Corporation) in the School of Biomedical Sciences, University of Nottingham was used. Peak lists were entered into MASCOT PMF (http://www.matrixscience.com/search_form_select.html) and ExPASy (http://www.expasy.org/tools/aldente/) database search engines.

Crypt/villus isolation. Intestinal epithelia were released from murine small intestine by incubation for 30 min at 4°C in PBS containing 2 mM EDTA as previously described (Sato et al., 2009), and immunoblots were performed as previously described (Nateri et al., 2005).

Survival curve. Kaplan–Meier survival analysis was used for *Fbxw7*$^{\Delta G}$*Apc*$^{Min/+}$ mice and their transgenic littermate (*Fbxw7*$^{fl/fl}$*Apc*$^{Min/+}$, Fbxw7$^{\Delta G}$) mice over a period of 62 wk (435 d; $n = 14$). The survival curve shows the percentage of mice remaining alive at 1-wk intervals. The x axis indicates times (in weeks) until mice were euthanized because of severe weight loss and anemia. 14 mice for each genotype group were used, and the survival curves were significantly different from each other ($P < 0.001$).

Cell culture, transfection, and cell cycle assays. Human CRC HCT116 and HEK293T cells were maintained in RPMI supplemented with 10% FBS. HCT116 cell lines harboring deletion of FBXW7 were a gift from A. Balmain (University of California, San Francisco, San Francisco, CA) and B. Vogelstein (Ludwig Center, Johns Hopkins University, Baltimore, MD; Mao et al., 2004a, 2008). Transfection of plasmids encoding FBXW7-α, -β, and -γ, DEK, GSK-3β, Tpm1-α (available from GenBank/EMBL/DDBJ under accession no. NM_000366), Luc, β-gal, GFP (control), or siRNA duplexes along with others was performed using Lipofectamine 2000 reagent (Invitrogen) according to the manufacturer's instruction. FLAG–GSK-3β plasmid was a gift from B.W. O'Malley (Baylor College of Medicine, Houston, TX; Wu et al., 2007), human DEK-GFP construct was a gift from J. Valcarcel (Centre de Regulació Genòmica, Barcelona, Spain) and A. Bürkle (University of Konstanz, Konstanz, Germany; Soares et al., 2006), and FLAG–Tpm1-α was a gift from J. Huot (Le Centre de recherche en cancérologie de l'Université Laval, Québec, Québec, Canada; Houle et al., 2007). To measure proliferation, HCT116 cells were transfected with an enhanced GFP expression vector (pC2-EGFP; Takara Bio Inc.) and/or with sequence scrambled controls and siDEK duplexes (Invitrogen) and peGFP-DEK vector. Transfection efficiency judged by enhanced GFP expression was 50–60%. 36 h after transfection, cells were collected by centrifugation, ethanol (70%) fixed, and treated with 50 μg DNase-free RNase/ml for 30 min, and DNA was stained with 50 μg propidium iodide/ml and analyzed by FACS. All assays were performed at least three times.

Cell migration, wound healing, and colony forming assays. Cell migration was measured using 24-well plates with polycarbonate membrane trans-well inserts with an 8-μm pore size (Corning). 2.5×10^4 cells were seeded, and cell migration was assessed after 24 h by fixing the cells attached to the lower surface in 10% methanol for 30 min. Cells were then stained with methylene blue and manually counted. Cell wound healing assays were performed in 6-well dishes. Cells were grown to >90% confluence and then starved in low serum media (0.1% serum in RPMI) for 24 h. A sterile 200-μl pipette tip was used to scratch three separate wounds. Healing across the wound line was assessed at 24 h. Images were analyzed using the ImageJ analysis program (National Institutes of Health), and the area of the wound was measured. For the wound healing assays, total pixel numbers with an intensity value of 0 were analyzed. All assays were performed at least three times in triplicate. Colony forming assay was performed using single cell suspensions, and 50 live cells (stained with Trypan blue) were plated in a 24-well precoated poly-L-lysine plate. After 2 d of incubation, single GFP^{+ve} cells and, after 7 d, colonies were identified for fluorescent microscopy experiments. Colonies were counted after 2 wk, and images were captured. Images were analyzed using the ImageJ analysis program, and the area of the colony was measured as outlined above. The experiments were repeated in triplicate and on two separate occasions.

Western blot analysis. Mice were sacrificed by cervical dislocation, and the intestines were removed and flushed extensively with cold PBS. The first 3 cm of the small intestine and large bowel were taken and homogenized in RIPA lysis buffer (Sigma-Aldrich) supplemented with protease inhibitor cocktail (Sigma-Aldrich). Immunoblots were performed as previously described (Nateri et al., 2005). Equal amount of total protein was denatured in the SDS sample loading buffer, separated on 8–16% SDS–polyacrylamide gradient gels, and transferred to polyvinylidene fluoride membranes, which were immunoblotted with various antibodies as indicated. Antibodies to polyclonal anti-Fbxw7 (Thermo Fisher Scientific and Invitrogen); cyclin E, c-Jun, p–c-JunS63, and p–c-MycT58/S62 (Cell Signaling Technology); DEK and β-actin (Abcam); and Notch 1 and Notch 4 (Santa Cruz Biotechnology, Inc.) were used. Antibodies to monoclonal GFP were obtained from Invitrogen, and antibodies to FLAG and hemagglutinin (HA) were obtained from Sigma-Aldrich. Western blot analysis for HCT116 and HEK293T cells was performed as previously described (Nateri et al., 2004). Cells were treated with LiCl (Sigma-Aldrich) and MG132 proteasome inhibitor (EMD) when required. The experiments were repeated on at least three separate occasions.

Co-IP and HA ubiquitination assay. Here we used 100 μl of anti-FLAG–conjugated agarose beads (Sigma-Aldrich) to immunoprecipitate Fbxw7 from whole cell extracts of the HEK293T cells using RIPA buffer (150 mM NaCl) with protease inhibitors. After IP, the beads were washed thoroughly with RIPA buffer adjusted to 500 mM. Immunoprecipitated proteins were eluted using 2× SDS loading buffer and then boiled at 95°C for 4 min. Denatured proteins were subsequently separated on 10% SDS PAGE and immunoblotted against anti-GFP and anti-HA antibodies as required after transferring to

polyvinylidene fluoride membranes as previously described (Wu et al., 2007). The experiments were repeated on at least two separate occasions.

Pulse-chase. HEK293T cells were transfected with DEK wild-type (DEK^{wt}) and/or DEK phosphorylation mutant ($DEK^{T15,67A}$ or DEK^{2A}) with Fbxw7-expressing plasmids. 30 h after transfection, cells were radioactively labeled for 3 h with 0.2 mCi [^{35}S]methionine and [^{35}S]cysteine/ml in a labeling medium lacking methionine and cysteine (ICN), followed by chase in complete medium with 1% FCS serum. Cell extracts and IP were performed with rabbit polyclonal antibody to GFP agarose-conjugated beads (Abcam) as previously described (Nateri et al., 2004).

Splicing efficiency assays. Activity of Luc and β-Gal proteins was measured using a Dual-Light reporter system (Applied Biosystems) according to the manufacturer's instruction. The reporter assays were performed in triplicates using a multifunction microplate reader (FLUOstar OPTIMA; BMG Labtech) after transient transfection of the bicistronic reporter along with plasmids encoding DEK, FBXW7-α, GSK-3β, and GFP (control) into HCT116 cells. For statistical analysis, the ratio of Luc activity to β-Gal was obtained from three independent experiments. Mean ± SD ($n = 3$; $P < 0.001$) values are shown. RT-PCR analysis of total RNA isolated from transfected cells represents an independent experiment but parallel to the reporter assay. DNA bands were derived from spliced and unspliced RNA.

Statistics. The significance of differences between mean and median was determined using the Student's *t* test and the Mann-Whitney *U* test, as appropriate. Significance testing was performed using SPSS version 15. Mean ± SD ($n = 3$; *, $P < 0.05$; **, $P < 0.01$; ***, $P < 0.001$) values are shown.

Online supplemental material. Fig. S1 shows the generation and characterization of intestinal (gut)-specific Fbxw7 knockout ($Fbxw7^{\Delta G}$) mice. Fig. S2 shows that intestinal targeted inactivation of *Fbxw7* leads to colonic and intestinal polyposis. Fig. S3 shows polyps and adenomas in $Apc^{Min/+}Fbxw7^{\Delta G}$ mice at an early age (3 wk old). Fig. S4 shows that a very small number and size of intestinal polyps/adenomas appeared from 3-wk-old $Apc^{Min/+}$ mice with β-catenin^{High} staining. Fig. S5 shows $Fbxw7^{\Delta G}$ lineage potential and elevation of Fbxw7 substrate expression upon depletion of Fbxw7 in mouse intestine. Fig. S6 shows IHC for c-Jun and FBXW7-α, -β, and -γ protein isoforms. Fig. S7 shows Western blot analysis of TPM protein expression upon overexpression of FBXW7s and phosphorylation of human DEK protein by GSK-3β. Fig. S8 shows cell growth regulation by human DEK and TPM1-α proteins. Table S1 lists primers used for genotyping and qRT-PCR. Table S2 lists TPM and DEK expression scores in sections from human colorectal tumor tissues with and without FBXW7 mutations. Table S3 shows the score quantification of TPM and DEK IHC performed in $FBXW7^{wt}$ and $FBXW7^{mut}$ human colorectal tumors. Online supplemental material is available at http://www.jem.org/cgi/content/full/jem.20100830/DC1.

We thank B. Vogelstein for providing HCT116 knockout cells, B.W. O'Malley, J. Valcarcel, and A. Bürkle for vectors, M. Ilyas, A. Grabowska, and C. Anbalagan for reading the manuscript, and E. Nye and P. Clarke for technical advice.

This study was supported by Cancer Research UK, research projects A9275 and A10247, and the University of Nottingham New Research Fund to A.S. Nateri.

No financial conflicts of interest exist.

Submitted: 27 April 2010
Accepted: 6 January 2011

REFERENCES

Akiyoshi, T., M. Nakamura, K. Yanai, S. Nagai, J. Wada, K. Koga, H. Nakashima, N. Sato, M. Tanaka, and M. Katano. 2008. Gamma-secretase inhibitors enhance taxane-induced mitotic arrest and apoptosis in colon cancer cells. *Gastroenterology*. 134:131–144. doi:10.1053/j.gastro.2007.10.008

Alexiadis, V., T. Waldmann, J. Andersen, M. Mann, R. Knippers, and C. Gruss. 2000. The protein encoded by the proto-oncogene DEK changes the topology of chromatin and reduces the efficiency of DNA replication in a chromatin-specific manner. *Genes Dev*. 14:1308–1312.

Allen, A., D.A. Hutton, and J.P. Pearson. 1998. The MUC2 gene product: a human intestinal mucin. *Int. J. Biochem. Cell Biol*. 30:797–801. doi:10.1016/S1357-2725(98)00028-4

Bharadwaj, S., and G.L. Prasad. 2002. Tropomyosin-1, a novel suppressor of cellular transformation is downregulated by promoter methylation in cancer cells. *Cancer Lett*. 183:205–213. doi:10.1016/S0304-3835(02)00119-2

Bonetti, P., T. Davoli, C. Sironi, B. Amati, P.G. Pelicci, and E. Colombo. 2008. Nucleophosmin and its AML-associated mutant regulate c-Myc turnover through Fbw7 γ. *J. Cell Biol*. 182:19–26. doi:10.1083/jcb.200711040

Brittan, M., and N.A. Wright. 2002. Gastrointestinal stem cells. *J. Pathol*. 197:492–509. doi:10.1002/path.1155

Carro, M.S., F.M. Spiga, M. Quarto, V. Di Ninni, S. Volorio, M. Alcalay, and H. Müller. 2006. DEK Expression is controlled by E2F and deregulated in diverse tumor types. *Cell Cycle*. 5:1202–1207. doi:10.4161/cc.5.11.2801

Cassia, R., G. Moreno-Bueno, S. Rodríguez-Perales, D. Hardisson, J.C. Cigudosa, and J. Palacios. 2003. Cyclin E gene (CCNE) amplification and hCDC4 mutations in endometrial carcinoma. *J. Pathol*. 201:589–595. doi:10.1002/path.1474

Crosnier, C., D. Stamataki, and J. Lewis. 2006. Organizing cell renewal in the intestine: stem cells, signals and combinatorial control. *Nat. Rev. Genet*. 7:349–359. doi:10.1038/nrg1840

Ekholm-Reed, S., C.H. Spruck, O. Sangfelt, F. van Drogen, E. Mueller-Holzner, M. Widschwendter, A. Zetterberg, and S.I. Reed. 2004. Mutation of hCDC4 leads to cell cycle deregulation of cyclin E in cancer. *Cancer Res*. 64:795–800. doi:10.1158/0008-5472.CAN-03-3417

el Marjou, F., K.P. Janssen, B.H. Chang, M. Li, V. Hindie, L. Chan, D. Louvard, P. Chambon, D. Metzger, and S. Robine. 2004. Tissue-specific and inducible Cre-mediated recombination in the gut epithelium. *Genesis*. 39:186–193. doi:10.1002/gene.20042

Fodde, R. 2002. The APC gene in colorectal cancer. *Eur. J. Cancer*. 38:867–871. doi:10.1016/S0959-8049(02)00040-0

Fre, S., M. Huyghe, P. Mourikis, S. Robine, D. Louvard, and S. Artavanis-Tsakonas. 2005. Notch signals control the fate of immature progenitor cells in the intestine. *Nature*. 435:964–968. doi:10.1038/nature03589

Fre, S., S.K. Pallavi, M. Huyghe, M. Laé, K.P. Janssen, S. Robine, S. Artavanis-Tsakonas, and D. Louvard. 2009. Notch and Wnt signals cooperatively control cell proliferation and tumorigenesis in the intestine. *Proc. Natl. Acad. Sci. USA*. 106:6309–6314. doi:10.1073/pnas.0900427106

Gooding, C., and C.W. Smith. 2008. Tropomyosin exons as models for alternative splicing. *Adv. Exp. Med. Biol*. 644:27–42. doi:10.1007/978-0-387-85766-4_3

Gunning, P.W., G. Schevzov, A.J. Kee, and E.C. Hardeman. 2005. Tropomyosin isoforms: divining rods for actin cytoskeleton function. *Trends Cell Biol*. 15:333–341. doi:10.1016/j.tcb.2005.04.007

Gupton, S.L., K.L. Anderson, T.P. Kole, R.S. Fischer, A. Ponti, S.E. Hitchcock-DeGregori, G. Danuser, V.M. Fowler, D. Wirtz, D. Hanein, and C.M. Waterman-Storer. 2005. Cell migration without a lamellipodium: translation of actin dynamics into cell movement mediated by tropomyosin. *J. Cell Biol*. 168:619–631. doi:10.1083/jcb.200406063

Helfman, D.M., P. Flynn, P. Khan, and A. Saeed. 2008. Tropomyosin as a regulator of cancer cell transformation. *Adv. Exp. Med. Biol*. 644:124–131. doi:10.1007/978-0-387-85766-4_10

Hershko, A., and A. Ciechanover. 1998. The ubiquitin system. *Annu. Rev. Biochem*. 67:425–479. doi:10.1146/annurev.biochem.67.1.425

Houle, F., A. Poirier, J. Dumaresq, and J. Huot. 2007. DAP kinase mediates the phosphorylation of tropomyosin-1 downstream of the ERK pathway, which regulates the formation of stress fibers in response to oxidative stress. *J. Cell Sci*. 120:3666–3677. doi:10.1242/jcs.003251

Jarriault, S., C. Brou, F. Logeat, E.H. Schroeter, R. Kopan, and A. Israel. 1995. Signalling downstream of activated mammalian Notch. *Nature*. 377:355–358. doi:10.1038/377355a0

Jenny, M., C. Uhl, C. Roche, I. Duluc, V. Guillermin, F. Guillemot, J. Jensen, M. Kedinger, and G. Gradwohl. 2002. Neurogenin3 is differentially

required for endocrine cell fate specification in the intestinal and gastric epithelium. *EMBO J.* 21:6338–6347. doi:10.1093/emboj/cdf649

Jensen, J., E.E. Pedersen, P. Galante, J. Hald, R.S. Heller, M. Ishibashi, R. Kageyama, F. Guillemot, P. Serup, and O.D. Madsen. 2000. Control of endodermal endocrine development by Hes-1. *Nat. Genet.* 24:36–44. doi:10.1038/71657

Kappes, F., C. Damoc, R. Knippers, M. Przybylski, L.A. Pinna, and C. Gruss. 2004. Phosphorylation by protein kinase CK2 changes the DNA binding properties of the human chromatin protein DEK. *Mol. Cell. Biol.* 24:6011–6020. doi:10.1128/MCB.24.13.6011-6020.2004

Kemp, Z., A. Rowan, W. Chambers, N. Wortham, S. Halford, O. Sieber, N. Mortensen, A. von Herbay, T. Gunther, M. Ilyas, and I. Tomlinson. 2005. CDC4 mutations occur in a subset of colorectal cancers but are not predicted to cause loss of function and are not associated with chromosomal instability. *Cancer Res.* 65:11361–11366. doi:10.1158/0008-5472.CAN-05-2565

Kennell, J., and K.M. Cadigan. 2009. APC and beta-catenin degradation. *Adv. Exp. Med. Biol.* 656:1–12. doi:10.1007/978-1-4419-1145-2_1

Kim, H., S. Eliuk, J. Deshane, S. Meleth, T. Sanderson, A. Pinner, G. Robinson, L. Wilson, M. Kirk, and S. Barnes. 2007. 2D gel proteomics: an approach to study age-related differences in protein abundance or isoform complexity in biological samples. *Methods Mol. Biol.* 371:349–391. doi:10.1007/978-1-59745-361-5_24

Koepp, D.M., L.K. Schaefer, X. Ye, K. Keyomarsi, C. Chu, J.W. Harper, and S.J. Elledge. 2001. Phosphorylation-dependent ubiquitination of cyclin E by the SCFFbw7 ubiquitin ligase. *Science.* 294:173–177. doi:10.1126/science.1065203

Kwak, E.L., K.H. Moberg, D.C. Wahrer, J.E. Quinn, P.M. Gilmore, C.A. Graham, I.K. Hariharan, D.P. Harkin, D.A. Haber, and D.W. Bell. 2005. Infrequent mutations of Archipelago (hAGO, hCDC4, Fbw7) in primary ovarian cancer. *Gynecol. Oncol.* 98:124–128. doi:10.1016/j.ygyno.2005.04.007

Mao, J.H., J. Perez-Losada, D. Wu, R. Delrosario, R. Tsunematsu, K.I. Nakayama, K. Brown, S. Bryson, and A. Balmain. 2004a. Fbxw7/Cdc4 is a p53-dependent, haploinsufficient tumour suppressor gene. *Nature.* 432:775–779. doi:10.1038/nature03155

Mao, J.H., M.D. To, J. Perez-Losada, D. Wu, R. Del Rosario, and A. Balmain. 2004b. Mutually exclusive mutations of the Pten and ras pathways in skin tumor progression. *Genes Dev.* 18:1800–1805. doi:10.1101/gad.1213804

Mao, J.H., I.J. Kim, D. Wu, J. Climent, H.C. Kang, R. DelRosario, and A. Balmain. 2008. FBXW7 targets mTOR for degradation and cooperates with PTEN in tumor suppression. *Science.* 321:1499–1502. doi:10.1126/science.1162981

Matsumoto, A., I. Onoyama, and K.I. Nakayama. 2006. Expression of mouse Fbxw7 isoforms is regulated in a cell cycle- or p53-dependent manner. *Biochem. Biophys. Res. Commun.* 350:114–119. doi:10.1016/j.bbrc.2006.09.003

Miyado, K., M. Kimura, and S. Taniguchi. 1996. Decreased expression of a single tropomyosin isoform, TM5/TM30nm, results in reduction in motility of highly metastatic B16-F10 mouse melanoma cells. *Biochem. Biophys. Res. Commun.* 225:427–435. doi:10.1006/bbrc.1996.1190

Mlakar, V., G. Berginc, M. Volavsek, Z. Stor, M. Rems, and D. Glavac. 2009. Presence of activating KRAS mutations correlates significantly with expression of tumour suppressor genes DCN and TPM1 in colorectal cancer. *BMC Cancer.* 9:282. doi:10.1186/1471-2407-9-282

Moberg, K.H., D.W. Bell, D.C. Wahrer, D.A. Haber, and I.K. Hariharan. 2001. Archipelago regulates Cyclin E levels in *Drosophila* and is mutated in human cancer cell lines. *Nature.* 413:311–316. doi:10.1038/35095068

Nakayama, K.I., and K. Nakayama. 2006. Ubiquitin ligases: cell-cycle control and cancer. *Nat. Rev. Cancer.* 6:369–381. doi:10.1038/nrc1881

Nasim, M.T., and I.C. Eperon. 2006. A double-reporter splicing assay for determining splicing efficiency in mammalian cells. *Nat. Protoc.* 1:1022–1028. doi:10.1038/nprot.2006.148

Nateri, A.S., L. Riera-Sans, C. Da Costa, and A. Behrens. 2004. The ubiquitin ligase SCFFbw7 antagonizes apoptotic JNK signaling. *Science.* 303:1374–1378. doi:10.1126/science.1092880

Nateri, A.S., B. Spencer-Dene, and A. Behrens. 2005. Interaction of phosphorylated c-Jun with TCF4 regulates intestinal cancer development. *Nature.* 437:281–285. doi:10.1038/nature03914

O'Neil, J., J. Grim, P. Strack, S. Rao, D. Tibbitts, C. Winter, J. Hardwick, M. Welcker, J.P. Meijerink, R. Pieters, et al. 2007. *FBW7* mutations in leukemic cells mediate NOTCH pathway activation and resistance to γ-secretase inhibitors. *J. Exp. Med.* 204:1813–1824. doi:10.1084/jem.20070876

Olson, B.L., M.B. Hock, S. Ekholm-Reed, J.A. Wohlschlegel, K.K. Dev, A. Kralli, and S.I. Reed. 2008. SCFCdc4 acts antagonistically to the PGC-1alpha transcriptional coactivator by targeting it for ubiquitin-mediated proteolysis. *Genes Dev.* 22:252–264. doi:10.1101/gad.1624208

Onoyama, I., R. Tsunematsu, A. Matsumoto, T. Kimura, I.M. de Alborán, K. Nakayama, and K.I. Nakayama. 2007. Conditional inactivation of *Fbxw7* impairs cell-cycle exit during T cell differentiation and results in lymphomatogenesis. *J. Exp. Med.* 204:2875–2888. doi:10.1084/jem.20062299

Phelps, R.A., S. Chidester, S. Dehghanizadeh, J. Phelps, I.T. Sandoval, K. Rai, T. Broadbent, S. Sarkar, R.W. Burt, and D.A. Jones. 2009. A two-step model for colon adenoma initiation and progression caused by APC loss. *Cell.* 137:623–634. doi:10.1016/j.cell.2009.02.037

Prasad, G.L., R.A. Fuldner, and H.L. Cooper. 1993. Expression of transduced tropomyosin 1 cDNA suppresses neoplastic growth of cells transformed by the ras oncogene. *Proc. Natl. Acad. Sci. USA.* 90:7039–7043. doi:10.1073/pnas.90.15.7039

Rajagopalan, H., P.V. Jallepalli, C. Rago, V.E. Velculescu, K.W. Kinzler, B. Vogelstein, and C. Lengauer. 2004. Inactivation of hCDC4 can cause chromosomal instability. *Nature.* 428:77–81. doi:10.1038/nature02313

Riccio, O., M.E. van Gijn, A.C. Bezdek, L. Pellegrinet, J.H. van Es, U. Zimber-Strobl, L.J. Strobl, T. Honjo, H. Clevers, and F. Radtke. 2008. Loss of intestinal crypt progenitor cells owing to inactivation of both Notch1 and Notch2 is accompanied by derepression of CDK inhibitors p27Kip1 and p57Kip2. *EMBO Rep.* 9:377–383. doi:10.1038/embor.2008.7

Sancho, R., A.S. Nateri, A.G. de Vinuesa, C. Aguilera, E. Nye, B. Spencer-Dene, and A. Behrens. 2009. JNK signalling modulates intestinal homeostasis and tumourigenesis in mice. *EMBO J.* 28:1843–1854. doi:10.1038/emboj.2009.153

Sato, T., R.G. Vries, H.J. Snippert, M. van de Wetering, N. Barker, D.E. Stange, J.H. van Es, A. Abo, P. Kujala, P.J. Peters, and H. Clevers. 2009. Single Lgr5 stem cells build crypt-villus structures in vitro without a mesenchymal niche. *Nature.* 459:262–265. doi:10.1038/nature07935

Schröder, N., and A. Gossler. 2002. Expression of Notch pathway components in fetal and adult mouse small intestine. *Gene Expr. Patterns.* 2:247–250. doi:10.1016/S1567-133X(02)00060-1

Shih, I.M., T.L. Wang, G. Traverso, K. Romans, S.R. Hamilton, S. Ben-Sasson, K.W. Kinzler, and B. Vogelstein. 2001. Top-down morphogenesis of colorectal tumors. *Proc. Natl. Acad. Sci. USA.* 98:2640–2645. doi:10.1073/pnas.051629398

Soares, L.M., K. Zanier, C. Mackereth, M. Sattler, and J. Valcárcel. 2006. Intron removal requires proofreading of U2AF/3′ splice site recognition by DEK. *Science.* 312:1961–1965. doi:10.1126/science.1128659

Spruck, C.H., H. Strohmaier, O. Sangfelt, H.M. Müller, M. Hubalek, E. Müller-Holzner, C. Marth, M. Widschwendter, and S.I. Reed. 2002. hCDC4 gene mutations in endometrial cancer. *Cancer Res.* 62:4535–4539.

Strohmaier, H., C.H. Spruck, P. Kaiser, K.A. Won, O. Sangfelt, and S.I. Reed. 2001. Human F-box protein hCdc4 targets cyclin E for proteolysis and is mutated in a breast cancer cell line. *Nature.* 413:316–322. doi:10.1038/35095076

Sundqvist, A., M.T. Bengoechea-Alonso, X. Ye, V. Lukiyanchuk, J. Jin, J.W. Harper, and J. Ericsson. 2005. Control of lipid metabolism by phosphorylation-dependent degradation of the SREBP family of transcription factors by SCF(Fbw7). *Cell Metab.* 1:379–391. doi:10.1016/j.cmet.2005.04.010

Tetzlaff, M.T., W. Yu, M. Li, P. Zhang, M. Finegold, K. Mahon, J.W. Harper, R.J. Schwartz, and S.J. Elledge. 2004. Defective cardiovascular development and elevated cyclin E and Notch proteins in mice lacking

the Fbw7 F-box protein. *Proc. Natl. Acad. Sci. USA*. 101:3338–3345. doi:10.1073/pnas.0307875101

Tsunematsu, R., K. Nakayama, Y. Oike, M. Nishiyama, N. Ishida, S. Hatakeyama, Y. Bessho, R. Kageyama, T. Suda, and K.I. Nakayama. 2004. Mouse Fbw7/Sel-10/Cdc4 is required for notch degradation during vascular development. *J. Biol. Chem*. 279:9417–9423. doi:10.1074/jbc.M312337200

Van der Flier, L.G., J. Sabates-Bellver, I. Oving, A. Haegebarth, M. De Palo, M. Anti, M.E. Van Gijn, S. Suijkerbuijk, M. Van de Wetering, G. Marra, and H. Clevers. 2007. The Intestinal Wnt/TCF Signature. *Gastroenterology*. 132:628–632. doi:10.1053/j.gastro.2006.08.039

van Es, J.H., M.E. van Gijn, O. Riccio, M. van den Born, M. Vooijs, H. Begthel, M. Cozijnsen, S. Robine, D.J. Winton, F. Radtke, and H. Clevers. 2005. Notch/gamma-secretase inhibition turns proliferative cells in intestinal crypts and adenomas into goblet cells. *Nature*. 435:959–963. doi:10.1038/nature03659

Varga, A.E., N.V. Stourman, Q. Zheng, A.F. Safina, L. Quan, X. Li, K. Sossey-Alaoui, and A.V. Bakin. 2005. Silencing of the Tropomyosin-1 gene by DNA methylation alters tumor suppressor function of TGF-beta. *Oncogene*. 24:5043–5052. doi:10.1038/sj.onc.1208688

Velcich, A., W. Yang, J. Heyer, A. Fragale, C. Nicholas, S. Viani, R. Kucherlapati, M. Lipkin, K. Yang, and L. Augenlicht. 2002. Colorectal cancer in mice genetically deficient in the mucin Muc2. *Science*. 295:1726–1729. doi:10.1126/science.1069094

Waldmann, T., I. Scholten, F. Kappes, H.G. Hu, and R. Knippers. 2004. The DEK protein—an abundant and ubiquitous constituent of mammalian chromatin. *Gene*. 343:1–9. doi:10.1016/j.gene.2004.08.029

Welcker, M., and B.E. Clurman. 2008. FBW7 ubiquitin ligase: a tumour suppressor at the crossroads of cell division, growth and differentiation. *Nat. Rev. Cancer*. 8:83–93. doi:10.1038/nrc2290

Welcker, M., A. Orian, J.E. Grim, R.N. Eisenman, and B.E. Clurman. 2004a. A nucleolar isoform of the Fbw7 ubiquitin ligase regulates c-Myc and cell size. *Curr. Biol*. 14:1852–1857. doi:10.1016/j.cub.2004.09.083

Welcker, M., A. Orian, J. Jin, J.E. Grim, J.W. Harper, R.N. Eisenman, and B.E. Clurman. 2004b. The Fbw7 tumor suppressor regulates glycogen synthase kinase 3 phosphorylation-dependent c-Myc protein degradation. *Proc. Natl. Acad. Sci. USA*. 101:9085–9090. doi:10.1073/pnas.0402770101

Wise-Draper, T.M., R.A. Mintz-Cole, T.A. Morris, D.S. Simpson, K.A. Wikenheiser-Brokamp, M.A. Currier, T.P. Cripe, G.C. Grosveld, and S.I. Wells. 2009. Overexpression of the cellular DEK protein promotes epithelial transformation in vitro and in vivo. *Cancer Res*. 69:1792–1799. doi:10.1158/0008-5472.CAN-08-2304

Wu, G., S. Lyapina, I. Das, J. Li, M. Gurney, A. Pauley, I. Chui, R.J. Deshaies, and J. Kitajewski. 2001. SEL-10 is an inhibitor of notch signaling that targets notch for ubiquitin-mediated protein degradation. *Mol. Cell. Biol*. 21:7403–7415. doi:10.1128/MCB.21.21.7403-7415.2001

Wu, R.C., Q. Feng, D.M. Lonard, and B.W. O'Malley. 2007. SRC-3 coactivator functional lifetime is regulated by a phospho-dependent ubiquitin time clock. *Cell*. 129:1125–1140. doi:10.1016/j.cell.2007.04.039

Yang, Q., N.A. Bermingham, M.J. Finegold, and H.Y. Zoghbi. 2001. Requirement of Math1 for secretory cell lineage commitment in the mouse intestine. *Science*. 294:2155–2158. doi:10.1126/science.1065718

Zheng, Q., A. Safina, and A.V. Bakin. 2008. Role of high-molecular weight tropomyosins in TGF-beta-mediated control of cell motility. *Int. J. Cancer*. 122:78–90. doi:10.1002/ijc.23025

Zhu, S., M.L. Si, H. Wu, and Y.Y. Mo. 2007. MicroRNA-21 targets the tumor suppressor gene tropomyosin 1 (TPM1). *J. Biol. Chem*. 282:14328–14336. doi:10.1074/jbc.M611393200